

THE CHAMP EXTENDED STELLAR SURVEY (CHESS): PHOTOMETRIC AND SPECTROSCOPIC PROPERTIES OF SERENDIPITOUSLY DETECTED STELLAR X-RAY SOURCES¹

K. R. COVEY^{2,3,4}, M. A. AGÜEROS^{2,5}, P. J. GREEN³, D. HAGGARD⁶, W. A. BARKHOUSE⁷, J. DRAKE³, N. EVANS³, V. KASHYAP³, D.-W. KIM³, A. MOSSMAN³, D. O. PEASE⁸, J. D. SILVERMAN⁹

DRAFT November 18, 2021

ABSTRACT

We present 348 X-ray emitting stars identified from correlating the Extended *Chandra* Multiwavelength Project (ChaMP), a wide-area serendipitous survey based on archival X-ray images, with the Sloan Digital Sky Survey (SDSS). We use morphological star/galaxy separation, matching to an SDSS quasar catalog, an optical color-magnitude cut, and X-ray data quality tests to create our catalog, the ChaMP Extended Stellar Survey (ChESS), from a sample of 2121 matched ChaMP/SDSS sources. Our cuts retain 92% of the spectroscopically confirmed stars in the original sample while excluding 99.6% of the 684 spectroscopically confirmed extragalactic sources. Fewer than 3% of the sources in our final catalog are previously identified stellar X-ray emitters. For 42 catalog members, spectroscopic classifications are available in the literature. We present new spectral classifications and H α measurements for an additional 79 stars. The catalog is dominated by main sequence stars; we estimate the fraction of giants in ChESS is $\sim 10\%$. We identify seven giant stars (including a possible Cepheid and an RR Lyrae star) as ChAMP sources, as well as three cataclysmic variables. We derive distances from $\sim 10 - 2000$ pc for the stars in our catalog using photometric parallax relations appropriate for dwarfs on the main sequence and calculate their X-ray and bolometric luminosities. These stars lie in a unique space in the L_X -distance plane, filling the gap between the nearby stars identified as counterparts to sources in the *ROSAT* All-Sky Survey and the more distant stars detected in deep *Chandra* and *XMM-Newton* surveys. For 36 newly identified X-ray emitting M stars we calculate $L_{H\alpha}/L_{bol}$. $L_{H\alpha}/L_{bol}$ and L_X/L_{bol} are linearly related below $L_X/L_{bol} \sim 3 \times 10^{-4}$, while $L_{H\alpha}/L_{bol}$ appears to turn over at larger L_X/L_{bol} values. Stars with reliable SDSS photometry have an ~ 0.1 mag blue excess in $u - g$, likely due to increased chromospheric continuum emission. Photometric metallicity estimates suggest that the sample is evenly split between the young and old disk populations of the Galaxy; the lowest activity sources belong to the old disk population, a clear signature of the decay of magnetic activity with age. Future papers will present analyses of source variability and comparisons of this catalog to models of stellar activity in the Galactic disk.

Subject headings: surveys — X-rays:stars — photometry:stars — spectroscopy:stars

1. INTRODUCTION

While X-ray source counterparts are now known to range from distant quasars to nearby active M dwarfs (e.g., Stocke et al. 1983, 1991; Schmitt et al. 1995; Zickgraf et al. 2003; Green et al. 2004; Anderson et al. 2007), X-ray data alone are frequently insufficient to determine unambiguously whether a given source is Galactic or extragalactic, or to make finer distinctions about its nature. Campaigns to find optical counterparts to X-ray sources have therefore been natural companions to

the creation of X-ray source lists since the days of the *Einstein Observatory*.

The Medium Sensitivity Survey (MSS; Gioia et al. 1984) and Extended Medium-Sensitivity Survey (Gioia et al. 1990) both required painstaking programs to identify counterparts to sources serendipitously detected in *Einstein* observations. To find counterparts to 63 of the 112 MSS sources, Stocke et al. (1983) obtained spectra for all of the optical objects inside or just outside the X-ray 90% confidence positional error circles—areas of radius $\sim 30''$ to $70''$. Once they found a plausible counterpart by comparing its f_X/f_V to that of similar objects detected in pointed *Einstein* observations, Stocke et al. (1983) continued to collect spectra until they reached objects at least four times fainter than the proposed counterpart or the ~ 20.5 mag limit of the Palomar Observatory Sky Survey (POSS). They found that $\sim 25\%$ of MSS sources were coronally emitting stars, primarily late-type dwarfs; they also found one cataclysmic variable (CV).

Similar efforts have been undertaken to identify some of the $\sim 125,000$ sources included in the *ROSAT* All-Sky Survey (RASS) Bright and Faint Source Catalogs (BSC and FSC; Voges et al. 1999, 2000). Only a relatively small fraction of RASS sources can be identified from correlations to existing databases. Bade et al.

¹ Observations reported here were obtained at the MMT Observatory, a joint facility of the Smithsonian Institution and the University of Arizona.

² The first two authors contributed equally to this study.

³ Harvard-Smithsonian Center for Astrophysics, 60 Garden Street, Cambridge, MA 02138

⁴ Spitzer Fellow

⁵ NSF Astronomy and Astrophysics Postdoctoral Fellow; Columbia University, Department of Astronomy, 550 West 120th Street, New York, NY 10027

⁶ NASA Harriett G. Jenkins Predoctoral Fellow, University of Washington, Department of Astronomy, Box 351580, Seattle, WA 98195

⁷ Physics Department, University of North Dakota, Grand Forks, ND 58202

⁸ Space Sciences Lab, 7 Gauss Way, Berkeley, CA 94720-7450

⁹ Max-Planck-Institut für extraterrestrische Physik, D-84571 Garching, Germany

(1998) found that 35% of the 80,000 RASS sources they considered had counterparts in SIMBAD and the NASA/IPAC Extragalactic Database. To identify other BSC sources, Bade et al. (1998) used objective prism spectra obtained as part of the Hamburg Quasar Survey (HQS; Hagen et al. 1995) and found candidate counterparts for 81.2% of the 3847 sources within the HQS footprint¹⁰. 155 (4%) are M stars, 136 (3.5%) K stars, and 4 (0.1%) F or G stars. Another 956 (24.9%) are saturated stars ($B \leq 14$ mag) for which no spectral class is available. There are also 31 white dwarfs (WDs; 0.8%) and 16 CVs (0.4%). There are uncertainties associated with these identifications, e.g., because of the resolution of the spectra ($R \approx 100$ at $H\gamma$). But the RASS/HQS program suggests that $\sim 33\%$ of the X-ray sources detected by *ROSAT* are Galactic stars, a result confirmed by later efforts (e.g., Zickgraf et al. 2003).

The *Chandra X-ray Observatory* and the *XMM-Newton X-ray Observatory* are both equipped with more sensitive X-ray detectors than *ROSAT* (albeit in different energy bands), but were designed primarily to conduct pointed observations. However, growing data archives have enabled a number of fairly deep, relatively small-area surveys, with X-ray source lists assembled and optical counterparts identified in much the same way as for the *Einstein* surveys. In addition, a few deep pencil-beam surveys have been completed with *Chandra* and *XMM-Newton*. Brandt & Hasinger (2005) compare the flux limits and solid angles for a number of these surveys; see their Figure 1.

The selection of optical counterparts for follow-up spectroscopy is generally simpler in these more recent surveys: the X-ray positional uncertainties are very small (typically less than $1''$ for *Chandra*). However, the focus of these surveys is often to characterize faint extragalactic X-ray emitters, and the stellar samples they provide are quite small.

For example, the *XMM* Bright Serendipitous Survey (BSS; Della Ceca et al. 2004) includes just under 400 sources. The BSS reaches a flux limit of $\sim 7 \times 10^{-14}$ erg $\text{cm}^{-2} \text{s}^{-1}$ in the 0.5 – 4.5 keV energy band for an area of 28.10 deg². 90% of the optical counterparts have magnitudes brighter than the POSS II limit of $R \sim 21$ mag (Della Ceca et al. 2004), and close to 90% of these counterparts now have spectra (López-Santiago et al. 2007). Of these, López-Santiago et al. (2007) identified 58 as stars, which therefore constitute $\sim 15\%$ of the X-ray counterparts—a smaller fraction than in the *Einstein* or *ROSAT* samples, but one which is consistent with the positions on the sky of the BSS fields, which are > 20 deg from the Galactic Plane. These authors compare the colors of their 58 stars to those predicted by the X-ray Galactic model XCOUNT (Favata et al. 1992). They find that model and data agree fairly well for the M stars in the sample but disagree rather dramatically for F, G, and K stars. They infer that the discrepancy is due to a stellar population currently absent from their model, possibly known X-ray emitting binaries such as RS CVn or BY Dra systems.

Feigelson et al. (2004) collected a smaller stellar sample from the *Chandra* Deep Field-North (CDF-N) survey.

The CDF-N has an area of ~ 448 arcmin²; individual exposures were as long as $\sim 2 \times 10^6$ s, resulting in a flux limit of 3×10^{-17} erg $\text{cm}^{-2} \text{s}^{-1}$ in the 0.5 – 2.0 keV band (Alexander et al. 2003). Of the ~ 500 sources in the CDF-N, only $\sim 3\%$ are stars, and Feigelson et al. (2004) use 11 of these to construct a statistically complete sample and study the evolution of X-ray properties. These stars belong primarily to an old-disk population (ages between 3 and 11 Gyr), and their X-ray properties are consistent with a faster-than-expected decline in magnetic activity ($\log L_X \propto t^{-2}$ rather than t^{-1} , where t is age; Feigelson et al. 2004).

Studies such as these would clearly benefit from a larger sample of X-ray emitting stars to analyze. The *XMM* Slew Survey (Freyberg et al. 2006), constructed from ≤ 15 s exposures as the satellite slewed, is one such survey. The recently released XMMSL1 catalog covers ~ 5800 deg² to a relatively shallow flux limit of 6×10^{-13} erg $\text{s}^{-1} \text{cm}^{-2}$ and includes 2692 sources in its “clean” version (Saxton et al. 2008). A search of the currently available XMMSL1 database finds that 410 *XMM* sources have a star cataloged in SIMBAD within $6''$, and it is clear that this program will eventually yield a large number of stellar X-ray sources. However, this stellar sample is still largely undefined. For example, re-matching the 410 sources to SIMBAD reveals that 35% have previously been identified as RASS sources. More work is necessary before we know exactly how many *new* stellar X-ray sources will come from this survey, or the similarly serendipitous 2XMM survey (Watson & XMM-Newton Survey Science Centre Consortium 2006).

We have collected the largest sample of stellar X-ray emitters in the field of the Galaxy identified and characterized to date from *Chandra* or *XMM* data. The X-ray data are from the Extended *Chandra* Multiwavelength Project (ChaMP), considerably easing the challenge of identifying the X-ray sources. *Chandra* provides sub-arcsecond astrometry over most of its field of view (Aldcroft et al. 2000), greatly facilitating unambiguous matching to optical counterparts, as does the lack of crowding at the high Galactic latitudes of the survey ($|b| > 20$ deg). In addition, the Extended ChaMP survey is designed to have significant overlap with the Sloan Digital Sky Survey (SDSS), which affords well-calibrated multi-color imaging and spectroscopy crucial both for elimination of extragalactic objects and for classification of stars.

We describe the ChaMP and SDSS in §2, and the process by which we identify candidate stellar counterparts in §3. In §4 we discuss the various tests we use to confirm that these candidates are in fact stellar X-ray emitters. In §5 we analyze the properties of our resulting sample of 348 X-ray emitting stars; we conclude in §6. Future work will analyze the X-ray variability of these stars and compare the properties of this catalog to stellar population models of the Galaxy incorporating evolution of time-dependent coronal X-ray emission.

2. THE SURVEYS

2.1. The Extended Chandra Multiwavelength Project

The *Chandra* Multiwavelength Project (ChaMP) is a wide-area serendipitous survey based on archival X-ray images of the $|b| > 20$ deg sky observed with

¹⁰ The unidentified sources are likely to be faint active galactic nuclei and clusters (Bade et al. 1998).

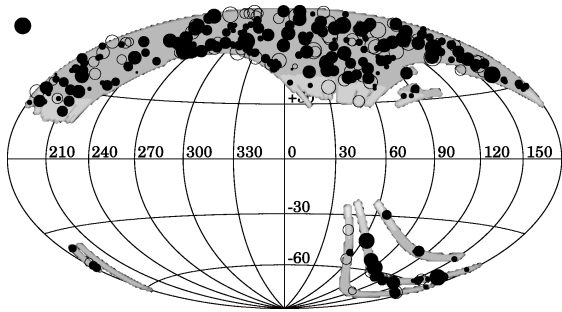


FIG. 1.— The Extended ChaMP footprint in Galactic coordinates. Open circles indicate fields observed with the ACIS-I detector, while filled circles indicate fields observed with the ACIS-S detector. The symbol size is proportional to the log of the exposure time; the symbol in the upper left corner corresponds to a 100 ksec exposure. The SDSS footprint is the shaded region.

the Advanced CCD Imaging Spectrometer (ACIS) on board *Chandra* (described in Weisskopf et al. 2002). The full 130-field Cycle 1–2 X-ray catalogs are public (Kim et al. 2004a, 2007a), and the most comprehensive X-ray number counts ($\log N$ - $\log S$) to date have been produced, thanks to 6600 sources and massive X-ray source-retrieval simulations (Kim et al. 2004b, 2007b). The simulations added one thousand artificial X-ray point sources across a wide range of fluxes to each actual *Chandra* ACIS image. The resulting images were subjected to the identical source detection and characterization as used for the actual survey, and a comparison of input and output properties allowed a full calculation of the ChaMP’s X-ray sky coverage and completeness as a function of e.g., source flux and off-axis angle (Kim et al. 2007b).

Green et al. (2004) used deep imaging ($r \sim 25$ mag) with the NOAO 4-m telescopes at KPNO and CTIO and follow-up spectroscopy with telescopes ranging from 1.5 to 10 m in diameter to obtain X-ray source identifications over 14 deg^2 of the Cycle 1–2 survey. 66 ChaMP fields were imaged in the g , r , and i bands; these data and photometric catalogs are available on the ChaMP webpage¹¹ (see also Barkhouse et al. 2008, in preparation). Optical spectra to $r \sim 22$ were obtained for as many objects as feasible in 27 prime fields, using primarily the WIYN 3.5 m on Kitt Peak, the MMT with the Blue Channel spectrograph on Mt Hopkins, Arizona, and the Magellan/Baade 6.5-m telescope with both the LRIS and IMACS spectrographs. A significant number of spectroscopic identifications were also obtained for $r \sim 18$ objects using the Fred Lawrence Whipple Observatory 1.5-m telescope with the FAST spectrograph. Green et al. (2004) classified 125 X-ray counterparts with optical spectroscopy. Of these, 90% are extragalactic in nature, as expected (63 are broad-line AGN). Silverman et al. (2008, in press) describe the spectroscopic effort in more detail in their paper on the AGN X-ray luminosity function, and a full ChaMP spectroscopic catalog is in preparation.

Given the need for even wider survey area to accumulate significant samples of rare objects, and the time-consuming nature of deep imaging and spectroscopy, the

ChaMP area has been extended to cover archival images from Cycles 1–6, but only to include *Chandra* images within the SDSS footprint (see §2.2). The Extended ChaMP now includes 392 ACIS fields covering a total area of roughly 33 deg^2 (see Figure 1) and catalogs $\sim 17,000$ X-ray sources¹². The median exposure time is 21 ksec, but individual exposures range from 1 to 119 ksec. Due to the low *Chandra* background rates, the formal statistical errors in net counts for each band are consistent within 2% of Poisson. Here we adopt the more conservative Gehrels (1986) prescription: $\sigma_{cts} = 1 + (N + 0.75)^{0.5}$.

SDSS photometry within about $20'$ of the aimpoint for each cataloged *Chandra* observation were obtained to cover the combined ACIS-I and ACIS-S fields of view¹³. Because the *Chandra* point spread function (PSF) increases with off-axis angle, comparatively few X-ray sources are detected beyond this radius and source centroids also tend to be highly uncertain. We note that some SDSS imaging strips do not completely cover the *Chandra* field of view. Detailed X-ray sky coverage vs. sensitivity maps represent a major ongoing effort of the ChaMP, described in Green et al. 2008 (in preparation), which will facilitate accurate volume-limit estimates and allow for e.g., luminosity function calculations and stellar population modeling.

While most ChaMP research to date has emphasized extragalactic objects (e.g., Silverman et al. 2005; Barkhouse et al. 2006; Kim et al. 2006, and Green et al. 2008, in preparation), the ChaMP lends itself well to stellar research. Compared to Galactic Plane studies, counterpart identification is very secure at the ChaMP survey’s high Galactic latitudes, crowded-field photometry is not an issue, and reddening is quite moderate. In addition, a more balanced ratio of thin/thick disk populations is sampled. However, the expected fraction of stellar X-ray sources detected in the ChaMP fields is relatively low: ChaMP fields, like those in the BSS, are away from the Plane and stars are on average weak X-ray emitters.

2.2. The Sloan Digital Sky Survey

The Sloan Digital Sky Survey (Fukugita et al. 1996; Gunn et al. 1998; Hogg et al. 2001; Smith et al. 2002; Gunn et al. 2006) is the deepest large-scale optical survey to date, and provides uniform photometric (to a depth of $r \sim 22.5$ and an accuracy of ~ 0.02 mag; Ivezić et al. 2004) and spectroscopic ($R \sim 1800$) datasets with which to identify ChaMP sources. The latest data release (DR6; Adelman-McCarthy et al. 2008) includes imaging for $\sim 9600 \text{ deg}^2$ and photometry for close to 3×10^8 unique objects. The SDSS spectroscopic footprint is smaller ($\sim 7400 \text{ deg}^2$); spectra over the $3800 - 9200 \text{ \AA}$ range are available for $> 10^6$ objects. The main spectroscopic samples are for galaxies with Petrosian $r < 17.77$ ($> 790,000$ objects) and quasars with PSF $i < 19.1$ ($> 100,000$ objects). The DR6 database also includes spectra for close to 300,000 stars, of which nearly 70,000

¹² Some of the weakest sources may be associated with, or contaminated by, cosmic-ray afterglows. Afterglows rarely affect brighter sources, or those with bright optical counterparts as in the current sample. See also §4.5.

¹³ For some observations, this was extended to a radius of $28'$ to achieve full coverage of the *Chandra* footprint.

¹¹ <http://hea-www.harvard.edu/CHAMP/>

are of spectral type M or later.

SDSS photometry and spectroscopy has been used to systematically identify RASS sources (e.g., Popesso et al. 2004; Anderson et al. 2007; Parejko et al. 2008, Agüeros et al. 2008, submitted). While the ChaMP is a very different survey from the RASS, the SDSS data are equally useful in identifying ChaMP sources, and particularly stellar sources. Typical classes of X-ray emitters, including coronally emitting stars, normal galaxies, quasars, and BL Lacs, have maximum X-ray-to-optical flux ratios corresponding to $\log(f_X/f_{opt})$ values of about -1 , 0 , $+1$, and $+1.5$ (e.g., Stocke et al. 1991; Zickgraf et al. 2003). Given the typical ChaMP $0.5-2$ keV flux¹⁴, $f_X = 10^{-14}$ erg cm⁻² s⁻¹, this implies that an optical counterpart for each of these categories of typical X-ray sources will be brighter than 19, 21, 24, and 25 mag, respectively. As a result, all but the very faintest stellar optical counterparts to ChaMP sources are bright enough to have confident SDSS photometric detections. Furthermore, such targets may be targeted for SDSS spectroscopy, allowing for secure identifications.

3. IDENTIFYING CANDIDATE STELLAR SOURCES

3.1. Matching To SDSS

We begin by searching the ChaMP catalog for sources with SDSS counterparts within $20''$ of each X-ray source centroid. We identify all potential SDSS matches to a ChaMP source and we record their distance from the X-ray centroid, along with a ratio of that distance to a radius characterizing the 95% X-ray position error. The latter depends on both the number of X-ray source counts and the *Chandra* off-axis angle (Kim et al. 2004a). We then inspect each X-ray source on the smoothed *Chandra* X-ray image and flag potentially contaminated sources, e.g. those that lie in the outskirts of bright X-ray sources. Detections that appear to be X-ray artifacts are also flagged, but not removed at this stage (see §4.5). Using the SDSS Image Tool (Nieto-Santisteban et al. 2004), we simultaneously create SDSS finders for each possible optical match to the X-ray source. Here again, contaminants and potential artifacts (saturation spikes, chip edges, high background regions, etc.) are noted.

During this visual inspection, a confidence rating is attached to each match from 0 to 3, with 3 being the highest confidence match. While we flag optically saturated objects during visual inspection, these are not rejected. A match confidence of 3 typically represents a single optical counterpart with a positional offset (X-ray to optical) no greater than $2''$ and/or less than the 95% X-ray position error.

We restrict our analysis here to ChaMP sources with a match confidence of 3 and SDSS counterparts with $r < 20.5$, a conservative estimate of the faintest magnitude for which SDSS performs robust morphological star/galaxy separation (see §4.2) even under poor observing conditions (Scranton et al. 2002). The resulting catalog contains 2121 ChaMP sources, of which 1320 are classified by SDSS as point sources.

¹⁴ This flux is the peak of an f_X histogram of ChaMP sources and corresponds approximately to a 50% completeness limit across the survey.

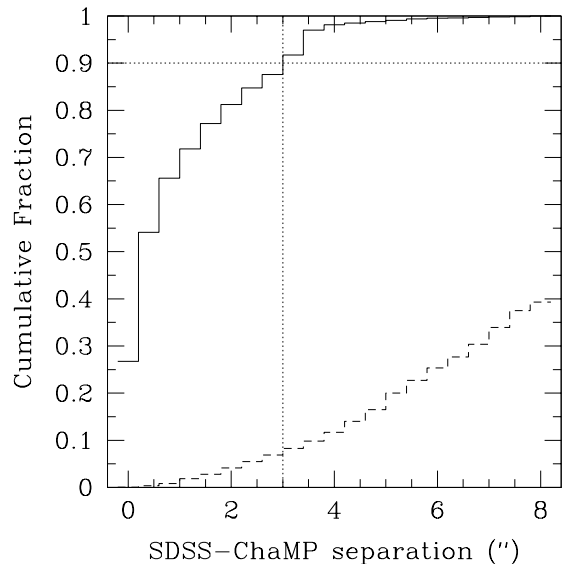


FIG. 2.— *Solid line*: Cumulative distribution of separations between X-ray and optical counterparts for real ChaMP/SDSS sources with $r < 20.5$ mag. *Dashed line*: Distribution of separations returned by matching shifted X-ray sources to catalog of SDSS objects with $r < 20.5$.

3.1.1. Estimating The Fraction Of Spurious SDSS Matches

We calculated the separation between the X-ray and optical positions of the 2121 matched objects selected in §3.1, finding a median X-ray/optical separation of $0.37''$ with $\sigma = 1.34''$. In Figure 2 we show the normalized cumulative histogram of these separations; 90% of the matched sources have positions in the X-ray and optical catalogs within $3''$ of each other.

We then shifted the X-ray source declinations by $+30''$ and searched for SDSS matches with $r < 20.5$ within $8''$ of these new positions, since only one of our original 2121 matched objects have separations larger than this. This procedure yields a control sample of 833 matches to these offset X-ray positions.

Figure 2 shows the (dashed) cumulative normalized histogram for this control sample; as expected, the cumulative fraction rises with separation. Note that the normalization used here is also 2121, so that the dashed histogram shows an upper limit to the fractional contamination of our sample by chance superpositions of independent X-ray and optical sources. At $3''$, the contamination is about 7%. At $4''$, an X-ray/optical separation larger than or equal to that for 99% of our sources, the contamination is about 12%. This represents a conservative upper limit, since no SDSS cuts other than $r < 20.5$ have been made.

3.2. Matching To 2MASS

The Two Micron All Sky Survey (2MASS) obtained near-infrared images of 99.998% of the sky between 1997 and 2001 (Skrutskie et al. 1997; Cutri et al. 2003; Skrutskie et al. 2006). The limiting (Vega-based) magnitudes for 10σ detections of point sources correspond roughly to $J = 15.8$, $H = 15.1$, and $K_s = 14.3$ mag. Positional uncertainties are $< 0.2''$.

We used the Gator interface¹⁵ to identify 2MASS counterparts for objects in our catalog, using a $3''$ matching radius centered on the X-ray/optical source's SDSS position. For objects with multiple 2MASS sources within $3''$, only the closest match was retained. This identified 2MASS counterparts for 889 of the 2121 objects in our initial catalog. We also performed a test similar to that described in §3.1.1 to estimate the likelihood of spurious SDSS/2MASS matches by applying a $30''$ offset to each source's SDSS position and then identifying 2MASS counterparts within $10''$. These false matches tend to have SDSS/2MASS separations of $7 - 9''$, with 90% lying outside of $3''$. The real matches, on the other hand, are all within $3''$; 97% are within $1''$.

4. CONFIRMING THE STELLAR SOURCES

4.1. ChaMP Spectroscopy

We queried the ChaMP spectroscopic database for existing observations and/or classifications of objects in our catalog. All of the spectra in the ChaMP database have been inspected and visually classified by members of the ChaMP collaboration as either AGN/QSOs, galaxies, or stars. 773 sources in our sample have high confidence classifications in the ChaMP spectroscopic database: of these, 92 have been classified as stellar sources, with the remaining 681 classified as extragalactic and possessing redshifts measured using the IRAF task *xcsoo*. These spectral classifications informed the criteria we develop to remove non-stellar contamination from our sample.

4.2. SDSS Star/Galaxy Separation

While SDSS provides automated morphological information for all objects it detects, many of the X-ray sources in our sample have optical counterparts significantly brighter than the SDSS saturation limit (~ 15 mag). The image flux distribution of saturated stars deviates strongly from a standard PSF and saturated stars are often classified as extended objects. To ensure accurate morphological classifications, we visually classified the 503 objects with $r < 18$. We identified 53 saturated stars misclassified as extended sources by the SDSS pipeline, and we adjusted their entries in our catalog.

We also checked the accuracy of the automated SDSS morphological classification by comparing the spectroscopic and photometric classifications of the 298 morphologically extended objects in our catalog with ChaMP spectra. All but five are classified spectroscopically as extragalactic: 115 are classified as galaxies and 176 as AGN/QSOs. Visual inspection of the SDSS images of these five objects reveals that three (CXOMP J143819.2+033349, J112740.4+565309, and J113311.9+010017) are extended galaxies, suggesting their spectroscopic classification as stars is erroneous. By contrast, CXOMP J142429.9+225641 and J235645.8-010138 are likely stars: they are only marginally resolved and may be either visual binaries or objects with photometric flaws resulting in morphological misclassification.

Of the 298 optically extended objects for which we have spectra, therefore, only two appear to be misclassified stars based on their photometry. This implies that

$\lesssim 0.7\%$ of the objects classified as extended by the SDSS photometric pipeline are actually point sources. Given this, we exclude from further analysis the 748 sources whose optical counterpart has been identified as extended by the pipeline. This increase in sample purity comes at the cost of excluding \sim five real point sources from our sample, which does not significantly affect our completeness.

Figure 3 presents the 1373 point sources in our initial catalog in various optical and infrared color-color and color-magnitude spaces. 475 of these point sources have spectroscopic classifications; 87 are identified as stars and 388 as extragalactic in nature. We highlight these two spectroscopic samples in Figure 3.

4.3. The SDSS Photometric QSO Catalog

The SDSS provides the largest, most uniform sample of photometrically selected quasars to $i < 21$, assembled using a nonparametric Bayesian classification based on kernel density estimation (Richards et al. 2004, 2006, 2007). Each object in the catalog is assigned a photometric redshift according to the empirical algorithm described by Weinstein et al. (2004); the difference between the measured color and the median colors of quasars as a function of redshift is minimized. The quasar catalog utilized in this work includes $\sim 10,000$ SDSS Data Release 5 (Adelman-McCarthy et al. 2007) photometrically selected QSOs that fall within $20'$ of a ChaMP field center (G. Richards, private communication, 2006; Green et al. 2008, in preparation). To minimize QSO contamination, we eliminate from consideration the 827 candidate stellar X-ray sources that are listed in the DR5 QSO catalog.

4.4. A Color-Magnitude Cut

While matching to the photometrically selected DR5 QSO catalog excludes the vast majority of QSOs in our sample, 47 of the remaining 546 stellar candidates are identified as QSOs in the ChaMP spectroscopic database. As the $g - i$ vs. i color-magnitude diagram (CMD) in Figure 3 shows, these QSOs are significantly fainter (≥ 2 mag) than spectroscopically confirmed stars with similar $g - i$ colors. This suggests that a color-magnitude cut can be used to separate stars from QSOs. However, 175 objects still under consideration at this stage are bright enough to saturate pixels in one or more of the five SDSS images, and their SDSS-based colors are untrustworthy.

We therefore restrict our final sample to the 363 sources whose optical counterparts are either flagged as SATURATED in the SDSS database (for a detailed discussion of the SDSS flags, see Stoughton et al. 2002) or are unsaturated and satisfy the $i < 16.2 + 0.7 \times (g - i)$ color-magnitude cut shown in Figure 3. Visual inspection confirms that the 27 objects that are saturated and do not meet our color-magnitude cut are in fact stars.

4.5. X-ray Quality Cuts

We now examine the X-ray properties of the 363 remaining ChaMP sources to identify potential contaminants.

- 27 sources are more than $12'$ from the *Chandra* optical axis and are subject to larger photometric and

¹⁵ <http://irsa.ipac.caltech.edu/applications/Gator/>

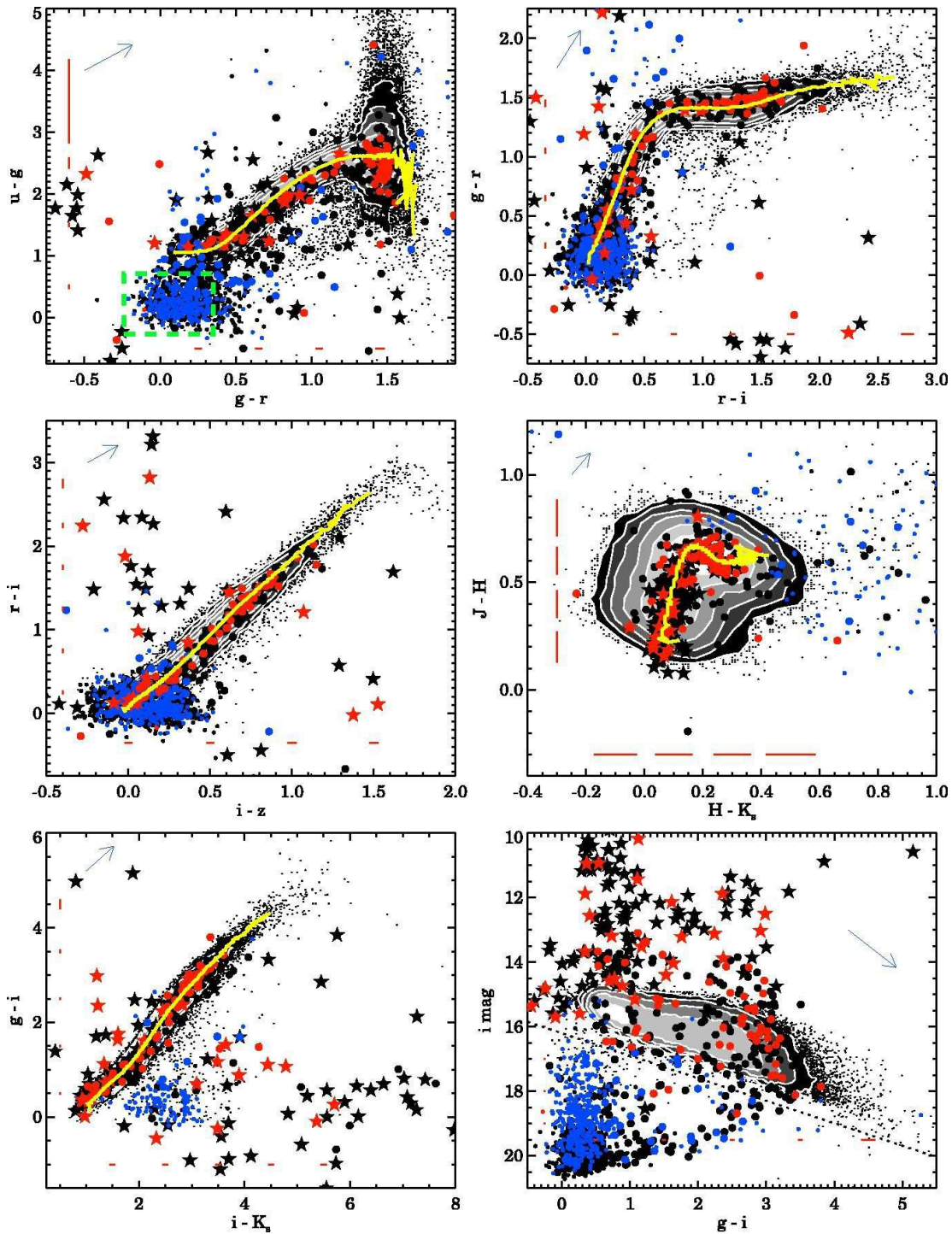


FIG. 3.— The location of our initial catalog in color-color and color-magnitude spaces. All 1373 ChaMP/SDSS point sources are shown as filled symbols, with stars and circles indicating saturated and unsaturated counterparts respectively. The 87 spectroscopically identified stars are red, while the 388 extragalactic sources are blue. Objects in the DR5 QSO catalog are shown with half-sized symbols; the green box in the upper left panel is the area of color space typically inhabited by $z < 2.5$ QSOs. Grayscale contours and black dots show the high quality sample of SDSS/2MASS point sources presented by Covey et al. (2007); the yellow line is the median color-color relation of this sample. The color-magnitude cut described in §4.4 to eliminate QSOs is shown as a dotted line in the i vs. $g-i$ CMD. Extinction vectors corresponding to $A_V = 1$ are shown with a blue arrow in the upper left corner of each color-color diagram, and in the upper right of the color-magnitude diagram. The red bars along each axis represent the typical photometric errors.

astrometric errors. Since almost all have a large number of counts, we preserve them in our sample. We do flag these sources in our final catalog, however, and we conservatively increase their X-ray flux errors by 50%.

- 16 sources are detected on ACIS S4, which suffers from increased noise and streaking relative to the other *Chandra* CCDs. These sources are flagged in our final catalog; we conservatively increase their X-ray flux errors by 20%.
- We find that 14 sources overlap according to the criteria of Kim et al. (2007a). For eight, the overlap is small (as defined by Kim et al. 2007a) and the X-ray photometry is reliable. For the other six, the overlap is large: we flag these sources in our catalog and conservatively double their X-ray flux errors.
- The exposure times for nine sources are typically less than half the maximum exposure time for their respective CCDs, indicating that the source extraction region encompasses an edge or gap. These sources have unreliable fluxes and we remove them from our sample.
- We checked a time-ordered list of photons inside the extraction region for each source in our catalog. We searched for two consecutive photons for which the chip coordinates are the same or differ by one pixel, the exposure frames (typically 3.2 s) increase by 1 or 2, and the energies decrease monotonically; these are features associated with cosmic ray afterglows¹⁶. We remove the three false sources (all with < 10 counts) we found in this manner from our catalog.

In summary, we remove 12 sources from our catalog based on their X-ray properties.

5. THE CHAMP/SDSS STELLAR CATALOG: CHSS

Imposing the criteria described above on our initial catalog of 2121 ChaMP detections results in a high confidence sample of 351 stellar X-ray emitters. This sample excludes 99.6% (681/684) of the spectroscopically identified extragalactic objects and includes 91% (81/89) of the spectroscopically identified stars. Of the eight spectroscopic stars eliminated from our sample, two lack SDSS counterparts with point source morphology, one is erroneously listed as having a photometric z in the SDSS QSO catalog, four fail to meet our color-magnitude cut, and one has an X-ray detection on the edge of a *Chandra* CCD. We discuss the six eliminated stars with point source SDSS counterparts in §5.2.

We remove the three remaining spectroscopically identified QSOs from our sample to produce a final catalog of 348 stellar X-ray emitters, which we define as the ChaMP Extended Stellar Survey (see Table 1 for a summary of the stages in the catalog construction). The 348 ChESS stars represent 17% of the ChaMP sources with SDSS counterparts, a fraction consistent with that found

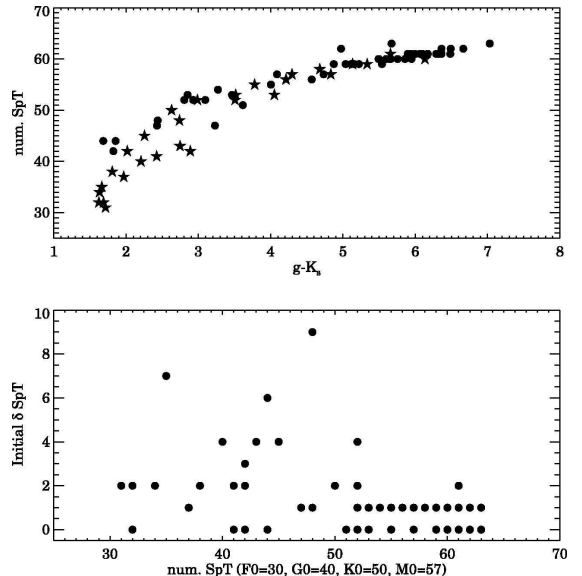


FIG. 4.— *Top panel:* Assigned spectral types as a function of $g - K_s$; saturated and unsaturated sources are shown as stars and circles respectively. *Bottom panel:* Initial spectral type uncertainty as a function of assigned type.

by López-Santiago et al. (2007), as expected. X-ray and optical/near-infrared properties of objects in this catalog are presented in Tables A1 and A2.

5.1. Previously Cataloged Stars

A number of ChESS stars are optically bright enough to have been previously cataloged. We search for entries in the SIMBAD catalog within $10''$ of the ChESS position for the 348 stars and find that 89 have matches. These stars are discussed in more detail in Appendix A.

The 89 stars can be divided into three groups. The largest group, 66 stars, is made up of optically bright stars that have yet to be identified as X-ray emitters. The first group’s natural complement is the small number of stars that have already been identified as X-ray sources; there are only 10 stars for which this is the case. The third group is of ChESS sources included in previous X-ray catalogs but not yet identified; there are 13 such sources. The vast majority of the objects in our catalog, therefore, represent new stellar identifications: previously known stellar X-ray sources make up $< 3\%$ of our sample.

5.2. Spectroscopic Stellar Sample

We used the Hammer (Covey et al. 2007), an Interactive Data Language code¹⁷ to obtain spectral types for the 81 stars in our sample for which we have spectra. The Hammer predicts the Morgan-Keenan (for stars earlier than M) or Kirkpatrick (for later stars) spectral type for a given star on the basis of a fit to a set of 30 spectral indices. In addition, the user can interactively modify the assigned spectral type. Employing this tool every spectrum was checked by eye and stars were assigned types independently by two authors (MAA, KRC). Cases where the types disagreed by more than two subclasses

¹⁶ For a description of this problem, see http://asc.harvard.edu/ciao/caveats/acis_caveats_071213.html.

¹⁷ Available from <http://www.cfa.harvard.edu/~kcovey/>.

TABLE 1
STAGES IN CATALOG CONSTRUCTION.

	Total Objects	Spectroscopic	
		Stars	Galaxies
Matched ChaMP/SDSS catalog	2121	89 (100%)	684 (100%)
Matched ChaMP/SDSS point sources	1373	87 (98%)	388 (57%)
... not in DR5 QSO catalog	546	86 (97%)	47 (7%)
... with $i < 16.2 + 0.7 \times (g - i)$	363 ^a	82 (92%)	3 (< 0.1%)
... with clean X-ray properties	351	81 (91%)	3 (< 0.1%)
Final catalog	348 ^b	81 (91%)	0 (0%)

NOTE. — Columns 3 and 4 give the number of spectroscopically confirmed stars and galaxies present in the catalog at each stage. The numbers in parentheses correspond to the fraction of the original number of these objects that is retained.

^aIncludes 27 saturated stars that do not meet this color-magnitude cut.

^bThree spectroscopically confirmed QSOs, and 11 sources with sub-standard X-ray detections are removed manually.

were reexamined. The spectral types ultimately assigned are in Table A3.

The top panel of Figure 4 shows the relationship between the assigned spectral types and each star’s $g - K_s$ color; the close relation between the two quantities (especially for unsaturated stars) suggests that the assigned types are accurate. As an additional test of this accuracy, we plot in the bottom panel of Figure 4 the difference between the two types initially assigned to each star. The mean difference is slightly more than one subclass, although the quality of the agreement is dependent on the spectral type of the star. The initial independent classifications for K and M class stars typically disagree by one subclass or less, while initial classifications for earlier F and G class stars typically disagree by 2 – 4 subclasses. We note that while eight of these stars have SIMBAD entries, only three have previously cataloged spectral types and only one is a previously known X-ray emitter. We identify CXOMP J025951.7+004619 as [BHR2005] 832–7, which we classify as an M5 star and which SIMBAD lists as an M5.5V star. CXOMP J122837.1+015720 is the known X-ray emitter GSC 00282–00187, classified as an M2 star; we have it as an M1 star. Finally, we identify CXOMP J231820.3+003129 as the F2 star TYC 577–673–1; SIMBAD lists this star as an F5.

We list $H\alpha$ equivalent widths (EqWs) for each star in Table A3, which we measure by dividing the line flux within a 20 Å window centered at 6563 Å with the continuum flux level determined from a linear fit to two regions (6503–6543 Å and 6583–6623 Å). We then use the χ factor (Walkowicz et al. 2004) to calculate $L_{H\alpha}/L_{bol}$ from these EqWs for the M stars with $H\alpha$ emission.

As mentioned above (§4.2), the cuts we use to identify a high confidence sample of stellar X-ray sources remove five spectroscopically confirmed stars from our catalog. CXOMP J114119.9+661006 and J234828.4+005406 are optically faint main sequence stars with spectral types K7 and M2 and are eliminated by our color-magnitude cut; we remove an M2 star, CXOMP J161958.8+292321, because its X-ray detection falls on the edge of a *Chandra* CCD. The remaining three sources are rarer cataclysmic variables, which frequently share color space with QSOs:

- SDSS J020052.2–092431 is a previously unknown CV. Follow-up optical observations are required to determine the nature of the system and its period. Its soft (0.5 – 2.0 keV) flux is $3.13 \pm 0.28 \times 10^{-14}$

ergs $\text{cm}^{-2} \text{s}^{-1}$, while its broadband (0.3–8.0 keV) flux is $9.04 \pm 0.65 \times 10^{-14}$ ergs $\text{cm}^{-2} \text{s}^{-1}$. This CV is eliminated by our color-magnitude cut.

- SDSS J150722.33+523039.8 was identified as a CV by Szkody et al. (2005). Follow-up photometry revealed that it is an eclipsing system with an extremely short orbital period of only 67 minutes. Furthermore, observations of systems with similarly broad absorption in the Balmer lines suggest that this CV may contain a pulsating WD (e.g., Woudt et al. 2004).

An initial match to the RASS did not return an X-ray counterpart to this CV (Szkody et al. 2005). It was the target of a *Chandra* observation that is included in ChaMP database. The CV’s soft flux is $2.36 \pm 0.84 \times 10^{-14}$ erg $\text{cm}^{-2} \text{s}^{-1}$, while its broadband flux is $7.33 \pm 1.81 \times 10^{-14}$ erg $\text{cm}^{-2} \text{s}^{-1}$. This CV is listed in the SDSS QSO catalog as having a non-zero z , and also is eliminated by our color-magnitude cut.

- SDSS J170053.29+400357.6 is a known X-ray emitting polar, in which the accretion stream flows directly onto the WD’s magnetic poles, with a period of 115 minutes (Szkody et al. 2003). Szkody et al. (2003) convert RASS counts into a flux assuming that for 2 keV bremsstrahlung spectrum, 1 count s^{-1} corresponds to a 0.1 – 2.4 keV flux of about 7×10^{12} ergs $\text{cm}^{-2} \text{s}^{-1}$. In this case, the resulting X-ray flux is $\sim 4.9 \times 10^{-13}$ ergs $\text{cm}^{-2} \text{s}^{-1}$. By contrast, the soft *Chandra* flux is $2.07 \pm 0.27 \times 10^{-13}$ ergs $\text{cm}^{-2} \text{s}^{-1}$, while its broadband flux is $6.81 \pm 0.62 \times 10^{-13}$ ergs $\text{cm}^{-2} \text{s}^{-1}$. This CV is eliminated by our color-magnitude cut.

For all three of these CVs, the broadband flux suggests there is a hard tail to the X-ray emission.

5.3. Giant Stars

In order to estimate the fraction of ChESS stars that is likely to be made up of evolved X-ray emitters, we generate simulated SDSS/2MASS observations using the TRILEGAL code (Girardi et al. 2005) and standard Galactic parameters. In Figure 5 we show the resulting J vs. $J - K_S$ CMD. Dwarf stars are defined as having surface gravities $\log g \geq 3.5$ and their distribution is shown by

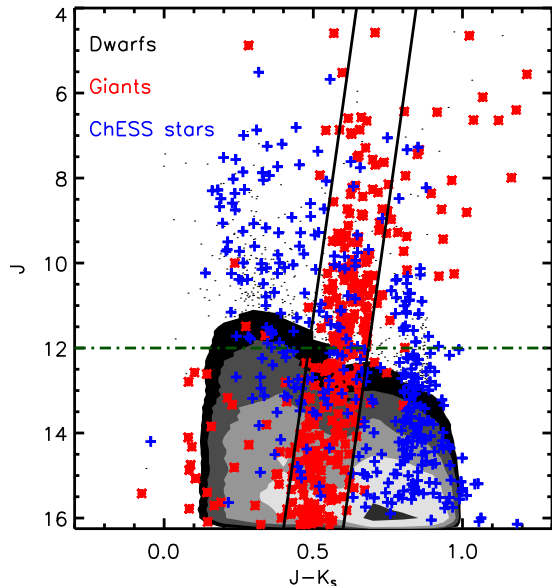


FIG. 5.— Simulated J vs. $J - K_S$ color-magnitude diagram, produced by the TRILEGAL galaxy model for SDSS/2MASS observations of a 10 deg^2 field, with the ChESS stars overplotted (blue plus signs). The contours and points correspond to the distribution of 10,254 dwarf stars ($\log g \geq 3.5$); 368 giants are highlighted as red asterisks. The solid lines enclose the area of the diagram in which giants are most populous. The green dot-dashed line is $J = 12$; fainter than this magnitude, giants make up only $\sim 10\%$ of the total number of stars, while brighter than this value they dominate the stellar population. We estimate that $\sim 10\%$ of the ChESS stars are giants.

the density contours and points. The positions of the simulated giant stars are given by red asterisks. TRILEGAL predicts that most giants (78%) should reside in a fairly narrow locus in J vs. $J - K_S$ color-magnitude space that stretches from $J \sim 4$ and $0.625 \leq J - K_S \leq 0.825$ down to $J \sim 16$ and $0.4 \leq J - K_S \leq 0.6$; we highlight this region of the CMD. We then plot the positions of the ChESS stars; 57 inhabit the giant region. However, the relative fraction of giants is not uniform across this region. For stars with $J > 12$ mag, giants represent no more than 11% of our simulated SDSS/2MASS detections, while they dominate the simulated stellar population at brighter magnitudes. Naively we would therefore only expect 3 of the 29 ChESS stars in the giant region with $J > 12$ to be giants; conversely, all 28 ChESS $J < 12$ stars in this region are strong giant candidates. Overall, this implies that $\sim 10\%$ of our sample is made up of giant stars. Our matching to SIMBAD, discussed in §5.1, identified five known luminosity class III and IV counterparts to ChaMP sources, as well as an RR Lyrae and a candidate Cepheid (see Appendix A), implying that the minimum fraction of ChESS giants is 2%.

5.4. Stellar Distances

We wish to derive distances for the ChESS stars using photometric parallax relations appropriate for dwarfs on the main sequence, since these dominate our sample. However, distance estimates based on SDSS photometry

are unreliable for the 175 saturated stars in our sample. Fortunately, the SDSS photometric pipeline identifies each object’s counterpart in the USNO-B catalog (Monet et al. 2003); similarly, 2MASS uses a $5''$ matching radius to identify counterparts in the Tycho 2 or USNO-A2.0 catalogs. As a result, we have either USNO or Tycho counterparts for 347 of the 348 stars in our sample.

We use the Tycho/USNO B magnitudes to construct $B - K_s$ colors for each source in the catalog and derive a relationship between $g - K_s$ and $B - K_s$ for the unsaturated stars:

$$g - K_s = 0.93 \times (B - K_s) + 0.25. \quad (1)$$

Comparisons of the synthetic $g - K_s$ obtained using Equation 1 to the measured $g - K_s$ for the unsaturated stars reveals that the synthetic $g - K_s$ color is accurate to within 0.3 mag (1σ), which we adopt as the characteristic uncertainty for our synthetic $g - K_s$.

We then generate synthetic $g - K_s$ for the 165 saturated SDSS stars with B magnitudes. We include in Table A2 the synthetic g predicted for each star (calculated from its synthetic $g - K_s$ and the observed K_s), as well as a saturation flag that indicates if a star is unsaturated, saturated in SDSS with a synthetic g from Tycho/USNO photometry, or saturated in SDSS and lacking a Tycho/USNO counterpart.

Finally, we use a preliminary fit to the M_{K_s} vs. $g - K_s$ CMD of Golimowski et al. (2008, in preparation), which agrees well with the tabulations of Kraus & Hillenbrand (2007), to derive distances to each star, using synthetic $g - K_s$ colors for stars with saturated SDSS photometry when possible. One star in our sample, CXOMP J153203.5+240501, is undetected in 2MASS, so we estimate its distance using a preliminary fit to the M_i vs. $g - i$ CMD of Golimowski et al. (2008).

The resulting distances are shown in Figure 6 as a function of $g - K_s$; formal uncertainties in these distances are $< 10\%$, but we adopt conservative uncertainties of 20% to account for potential systematic errors in the underlying parallax relations. An estimate of the distance limit imposed by the i vs. $g - i$ cut described in §4.4, calculated as a function of $g - K_s$ via the color-magnitude data tabulated by Kraus & Hillenbrand (2007), is shown in Figure 6 as a dashed line. This limit matches the observed upper envelope of the ChESS catalog well. The optical/near-infrared CMD cut imposes implicit distance limits of between 2000 and 1000 pc for G and K stars and of 1000 to 200 pc for stars with spectral types M0 to M6.

Five stars in the ChESS catalog have formal distance estimates placing them within 20 pc; all five have SIMBAD counterparts. Two, CXOMP J080500.8+103001 and J144232.8+011710, are identified as giant stars, rendering our main sequence distance estimates invalid. Two others, CXOMP J171954.1+263003 and J171952.9+263003, appear to be members of a binary system, despite rather different photometric distance estimates (8.2 and 5 pc); a trigonometric parallax has been derived for the brighter component (J171954.1+263003/V647 Her), placing the system at a distance of 12 pc. The last of the five, CXOMP J080813.5+210608/LHS 5134, is also likely to be nearby: it is identified in SIMBAD as an M2.5 star, with a distance estimate of ~ 10 pc from spectroscopic parallax.

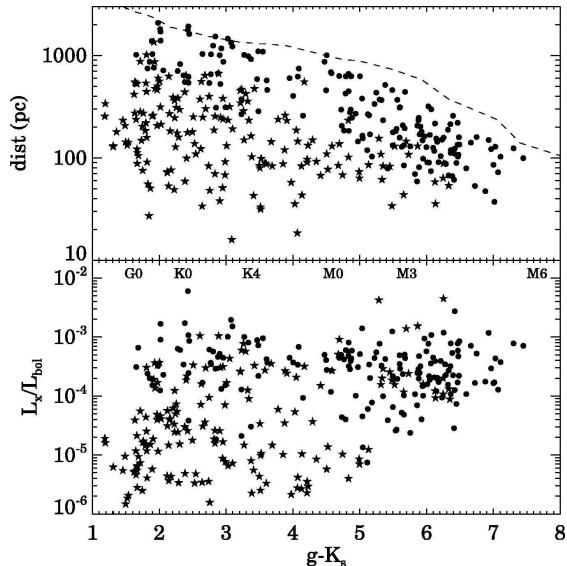


FIG. 6.— *Top Panel:* The distance to ChESS stars as a function of $g - K_s$ color. Stars with unsaturated SDSS photometry and clean X-ray detections are shown as points; those with saturated SDSS photometry and/or flagged X-ray detections are shown as stars. The dashed line is the distance limit imposed by the i vs. $g - i$ CMD cut described in §4.4. *Bottom Panel:* L_X/L_{bol} as a function of $g - K_s$.

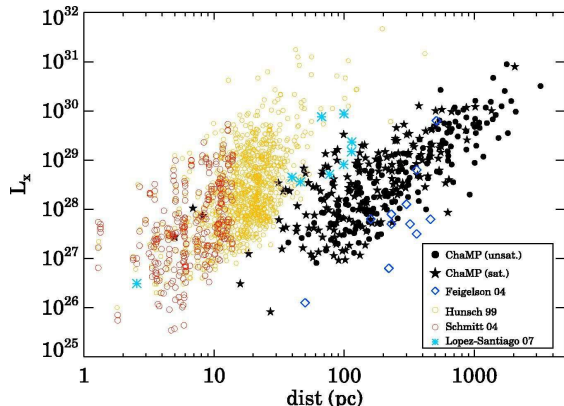


FIG. 7.— L_X as a function of distance for several samples of X-ray emitting stars. ChESS stars with unsaturated SDSS photometry and clean X-ray detections are shown as filled circles; those with saturated SDSS photometry and/or flagged X-ray detections are shown as stars. Also shown are the samples of Schmitt & Liefke (2004) (red circles), Hünsch et al. (1999) (yellow circles), Feigelson et al. (2004) (blue diamonds), and López-Santiago et al. (2007) (cyan asterisks).

5.5. Stellar X-ray Luminosities

Having estimated the distances to our stars, we determine their X-ray luminosities using both the soft (0.5 – 2.0 keV) and broadband (0.5 – 8 keV) ChaMP fluxes, whose construction is described in Kim et al. (2007a)¹⁸. The resultant L_X values are included in Ta-

ble A1; here we limit our discussion to soft X-ray luminosities for comparison purposes. These luminosities are shown in Figure 7 as a function of distance, along with data from several other catalogs of stellar X-ray emitters. The primary source of the comparison data presented here is *ROSAT*: we include the Schmitt & Liefke (2004) and Hünsch et al. (1999) catalogs (0.1 – 2.4 keV luminosities). We also include the 11 stars identified by Feigelson et al. (2004) in the CDF-N (0.5 – 2 keV) and the nine stars in the López-Santiago et al. (2007) *XMM* BSS sample (0.5 – 4.5 keV) for which they provide distances. Compared to these surveys, the ChESS catalog samples a unique area in the L_X –distance plane, covering the ranges of $2 \times 10^{26} \lesssim L_X \lesssim 2 \times 10^{31}$ ergs s⁻¹ and $30 \lesssim d \lesssim 3000$ pc.

The ChESS stars are for the most part more luminous than those in the volume complete sample assembled by Schmitt & Liefke (2004). Despite their low intrinsic luminosities, the nearest stars have moderately large X-ray fluxes ($\sim 10^{-12}$ ergs cm⁻² s⁻¹). Fields in the *Chandra* archive including such sources are explicitly excluded from the ChaMP survey: the increased likelihood of saturation in X-ray and optical imaging reduces the ability to detect and classify other X-ray sources in the field, and greatly complicates the calculation of the effective area sampled by the observation.

The larger catalog of stellar X-ray emitters assembled by Hünsch et al. (1999) provides a more natural comparison to our ChESS catalog. The L_X lower limit of each sample increases with distance, as expected for flux-limited catalogs. While the distance limit of the ChESS catalog is fundamentally optical in nature (due to the CMD cut described in §4.4), a crude comparison of the relative sensitivities of the surveys can be made by comparing the distances to which each instrument can detect stars of a given L_X : the Hünsch et al. (1999) sample includes stars with $L_X = 10^{28}$ ergs s⁻¹ to a distance of 30 pc, while the ChESS catalog contains such stars out to 200 pc. The surface density of stars in the ChESS catalog (~ 10 deg⁻²) exceeds that of the Hünsch et al. (1999) catalog (3×10^{-4} deg⁻²) by nearly five orders of magnitude.

Figure 7 shows that the ChESS stars’ properties are most similar to those of stars included in other *Chandra* and *XMM* catalogs. These catalogs are not interchangeable, however. For example, while the luminosities of the Feigelson et al. (2004) CDF-N stars are comparable to those of the least luminous members of the ChESS catalog, that sample’s effective distance limit is beyond that of the ChESS catalog for equivalent X-ray luminosities. Conversely, because the López-Santiago et al. (2007) sample relies on trigonometric parallax measurements for distances, these *XMM*-detected stars, while also comparably X-ray luminous to the ChESS stars, make up a shallower sample.

We also present in Table A1 the hardness ratio (HR) for each source, where $\text{HR} = (H_c - S_c)/(H_c + S_c)$ and H_c and S_c are the number of hard and soft counts, respectively (Kim et al. 2007a). The stars in our catalog are quite soft, with typical HRs from -1.0 to -0.6 ; HR shows no clear correlation with L_X or $g - K_s$.

¹⁸ Note that this conversion assumes a $\Gamma = 1.7$ power-law X-ray spectrum; variations in coronal temperature and metallicity can produce count to flux conversion factors that differ by a factor of

two.

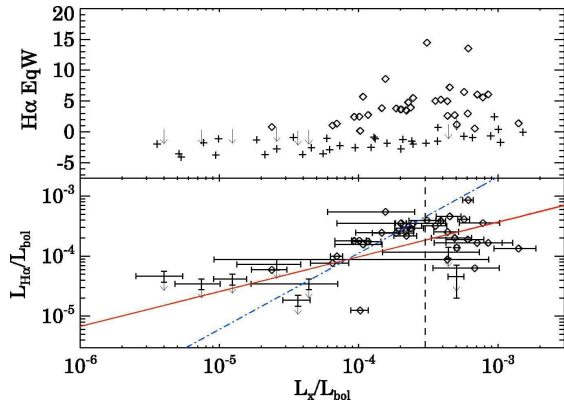


FIG. 8.— *Top Panel:* $H\alpha$ EqW vs. L_X/L_{bol} for stars with ChaMP spectra. Negative EqWs indicate the presence of absorption lines. F, G, and K stars are shown with plus signs; M stars are indicated with diamonds. The downward-pointing arrows indicate the EqW upper limits for M stars with no detected $H\alpha$ emission. *Bottom panel:* $L_{H\alpha}/L_{bol}$ vs. L_X/L_{bol} for the M stars in the spectroscopic sample, with symbols as above. The red line is the best fit relation between $L_{H\alpha}/L_{bol}$ and L_X/L_{bol} for the entire sample. The blue-dot dashed line is the relation for the stars with $L_X/L_{bol} < 3 \times 10^{-4}$, a value indicated by the dashed line.

5.6. Stellar Bolometric Luminosities

For each star, we derive the bolometric luminosity using the $g - K_s$ color and the appropriate Kraus & Hillenbrand (2007) bolometric correction. The resulting L_X/L_{bol} ratios are presented in Table A1 and shown in the bottom panel of Figure 6 as a function of $g - K_s$.

The lower limit to the L_X/L_{bol} values in the ChESS catalog is shaped by the sample’s effective L_X limit, which is a function of the exposure times of the *Chandra* images used to build the ChaMP. The presence of an upper envelope at $L_X/L_{bol} \sim 10^{-3}$, however, reflects a physical characteristic of the stars. Previous investigators have found a similar empirical upper limit to the efficiency of stellar X-ray emission (e.g., Vilhu & Rucinski 1983; Vilhu 1987; Herbst & Miller 1989; Stauffer et al. 1994). While the cause of this so-called saturation is still unknown, it is most commonly attributed to feedback processes that quench the efficiency of the stellar dynamo and/or the ability of the dynamo to heat the coronal plasma (Collier Cameron & Jianke 1994), or to centrifugal stripping of the coronal plasma at the high rotational velocities associated with large L_X (Jardine 2004).

Figure 8 compares non-simultaneous measures of the strength of the $H\alpha$ emission line, a common diagnostic of chromospheric activity, with L_X/L_{bol} , a tracer of coronal activity for stars in our spectroscopic sample. Similar measurements from M stars in young clusters and the solar neighborhood (e.g., Reid et al. 1995), have found $L_X = (3 - 5) \times L_{H\alpha}$, but were typically made using *ROSAT* data. As stellar coronae produce very soft X-ray emission, it is unsurprising that the ChESS data, measuring harder X-rays, produces an L_X/L_{bol} ratio of $\sim 2/3$, lower than the *ROSAT*-measured ratio by a factor of five.

The correlation between L_X/L_{bol} and $L_{H\alpha}/L_{bol}$ in

the ChESS data, however, is highly significant by Cox Proportional Hazard ($P = 0.0008$), Kendall’s τ ($P = 0.0027$), and Spearman’s ρ tests ($P = 0.0064$), as implemented in the Astronomy Survival Analysis Package (Lavalley et al. 1992). We perform bivariate linear regressions with $\log(L_X/L_{bol})$ as the dependent variable, using the parametric EM algorithm, and find the following best-fit relationship:

$$\log(L_{H\alpha}/L_{bol}) = (0.58 \pm 0.13) \times \log(L_X/L_{bol}) - (1.69 \pm 0.48) \quad (2)$$

with RMS residuals of 0.39; this relationship is shown as the red line in Figure 8. When restricting the sample to $L_X/L_{bol} < 3 \times 10^{-4}$, the best-fit regression line steepens to:

$$\log(L_{H\alpha}/L_{bol}) = (1.27 \pm 0.24) \times \log(L_X/L_{bol}) + (1.13 \pm 0.94), \quad (3)$$

shown as the blue dot-dashed line in Figure 8, with RMS residuals of 0.31.

The steepening of the L_X/L_{bol} vs. $L_{H\alpha}/L_{bol}$ relation when high L_X/L_{bol} sources are excluded, and the turnover in $L_{H\alpha}/L_{bol}$ at large L_X/L_{bol} that is clearly visible in Figure 8, reveal that stars with very active coronae can possess very pedestrian chromospheres, at least when viewed at distinct epochs. To ensure that this effect is not merely an effect of uncertain $H\alpha$ measurements in low S/N spectra, we visually inspected the $H\alpha$ region in the stars with $L_X/L_{bol} > 3 \times 10^{-4}$. We find that these spectra are of high enough quality to confirm that only very low levels of $H\alpha$ emission are present in these stars. We also verified that there are no significant differences in the spectral type or Galactic height of stars when the sample is divided at $L_X/L_{bol} = 3 \times 10^{-4}$.

There exist at least two plausible explanations for this seeming disconnect between the chromospheric and coronal properties of the stars with the most active coronae:

1. Our X-ray selected sample is biased towards detecting flaring stars, whose non-simultaneous optical spectra may be obtained when the star has returned to quiescence. The seeming disconnect between the coronal and chromospheric properties would then simply reflect the temporal disconnect in the observations of these stars. If this is the case, an extremely crude indicator of the duty cycle of X-ray flares on M stars in the Galactic disk can be derived from the $\sim 45\%$ (19/43) of the sample with low, and presumably quiescent, $H\alpha$ luminosity: the failure to observe significant $H\alpha$ emission during spectroscopic exposures with a median length of 720 s would imply an upper limit on the typical flare rate of 5 $H\alpha$ flares hr^{-1} .
2. Alternatively, the lack of correlation between chromospheric and coronal emission may be a sign that these two types of activity decouple as coronal activity levels approach the saturated regime. This hypothesis has been advanced previously (e.g., Cram 1982; Pettersen 1987; Mathioudakis & Doyle 1989; Houdebine et al. 1996); in this scenario, the relative efficiencies of radiative processes that cool the corona and chromosphere (e.g., $H\alpha$, Ca II, and

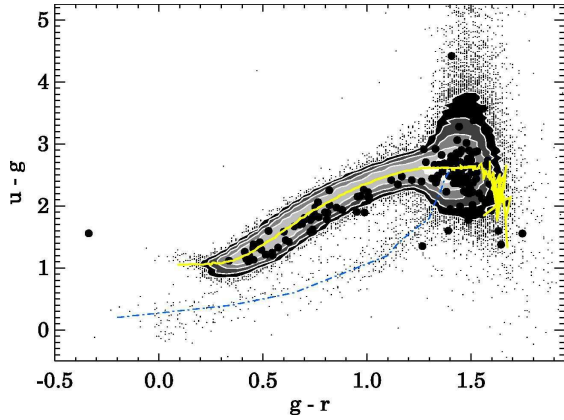


FIG. 9.— $u-g$ vs. $g-r$ for the ChESS stars with unsaturated SDSS photometry and unflagged X-ray detections (dots) with the optically selected SDSS/2MASS sample constructed by Covey et al. (2007) shown for comparison, as in Figure 3. The yellow line is the median stellar colors of the Covey et al. (2007) sample; the blue dashed line shows the locus of WD/M dwarf pairs identified by Smolčić et al. (2004).

Mg emission, highly ionized X-ray line emission, and ultraviolet continuum emission) are sensitive to the strength of stellar activity. To explain the effect seen here, extreme levels of stellar activity would have to quench cooling of the chromosphere via $H\alpha$ emission even as the corona continues to be cooled efficiently by X-rays.

The relatively weak coronae implied by the $L_X/L_{H\alpha}$ relationship measured from the low-activity portion of our sample and its apparent breakdown at high activity levels present intriguing clues to the temporal behavior of coronal activity over timescales characteristic of both the non-simultaneity effects ($t < 10$ yr) and population effects ($t > 1$ Gyr) discussed above. The current sample of stars with measurements of both L_X/L_{bol} and $L_{H\alpha}/L_{bol}$ is too small, however, to draw firm conclusions. We defer a full analysis of these effects to follow-up studies.

5.7. Stellar Colors

While the clearest signatures of magnetic activity are spectroscopic in nature, stellar activity can impact a star’s broadband colors as well. In particular, magnetically active stars appear to possess ultraviolet (UV) excesses of $0.03 - 0.1$ mag in $U - B$ compared to non-active stars. This excess has been attributed to continuum emission generated from hot, active chromospheres (Houdebine et al. 1996; Houdebine & Stempels 1997; Amado & Byrne 1997; James et al. 2000; Sung et al. 2002; Amado 2003; Bochanski et al. 2007).

The $u-g$ vs. $g-r$ color-color diagram in Figure 9 shows evidence for a similar shift, with X-ray emitting, optically unsaturated ChESS stars lying systematically lower than the median $u-g$ vs. $g-r$ locus measured by Covey et al. (2007) from a sample of optically selected SDSS/2MASS stars. This shift in color-color space, however, is not unambiguous proof of a $u-g$ excess, as the offset could be caused by a red excess in $g-r$, particularly since active stars can have strong $H\alpha$ emission that contributes additional flux to the r band. Our spectroscopic sample, however, does not include any stars

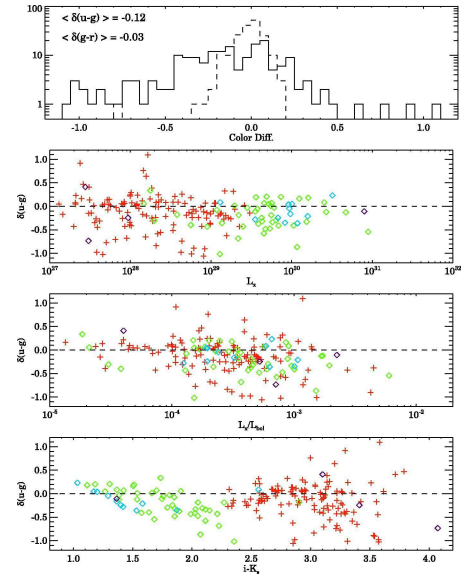


FIG. 10.— *Top Panel:* Histograms of color differences between unsaturated ChESS stars and optically selected stars with identical $i-K_s$. Differences for $u-g$ (solid line) and $g-r$ (dashed line) are shown. *Second Panel:* $u-g$ differences for unsaturated stars as a function of L_X . M stars are shown as red crosses, while F, G, and K stars are shown as purple, blue, and green diamonds respectively. *Third Panel:* $u-g$ differences for unsaturated stars as a function of L_X/L_{bol} . *Bottom Panel:* $u-g$ differences for unsaturated stars as a function of $i-K_s$.

with $H\alpha$ equivalent widths significantly larger than 10 \AA (see Table A3), and even such strong $H\alpha$ emission lines contribute only a small fraction to the flux transmitted through a $\sim 1000\text{-\AA}$ wide filter, brightening a star in the r band by only 0.01 mag.

To confirm that the offset in $u-g$ vs. $g-r$ is due to the stars’ anomalous $u-g$ colors, we compare the offsets between the $u-g$ and $g-r$ colors of unsaturated stars in our sample and the median colors of non-active stars with the same $i-K_s$ color tabulated by Covey et al. (2007) (see top panel, Figure 10). While the spread is large, active stars are systematically bluer by 0.12 mag in $u-g$ than inactive stars. By contrast, the $g-r$ colors of active stars are consistent with those of inactive stars to within 0.03 mag, and there the difference is that active stars are bluer than inactive stars. This is inconsistent with the idea of a red shift caused by the addition of $H\alpha$ emission into a star’s r band.

While stellar $u-g$ colors are sensitive to metallicity and the presence of unresolved WD companions, neither effect is likely to explain the offset seen here. The sensitivity of $u-g$ to metallicity is due to line blanketing, where absorption by a large number of metal lines in the u band leads to preferentially redder $u-g$ colors for more metal-rich stars. Interpreted as a metallicity effect, however, the ~ 0.1 mag blue $u-g$ offset implies that X-ray luminous stars have metallicities more than half a dex lower than the standard field population (Karaali et al. 2005), exceedingly unlikely given the well known link between stellar age and X-ray luminosity.

Similarly, while main sequence stars with an unresolved WD companion have anomalously blue $u-g$ colors, as well as the potential for enhanced X-ray lumi-

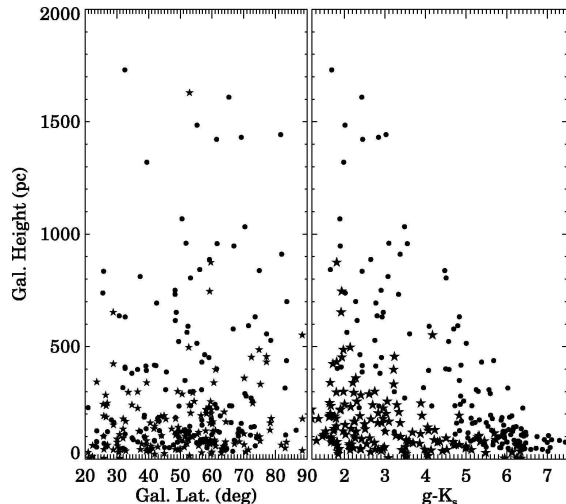


FIG. 11.— *Left Panel:* Height in the Galactic disk (in pc) as a function of Galactic latitude. *Right Panel:* Height in the Galactic disk (in pc) as a function of $g-K_s$. Symbols as in Fig. 7.

nosity, the colors of the stars in our sample disagree with those expected for such binaries. The SDSS colors of WD/main sequence binaries found by Smolčić et al. (2004) and Silvestri et al. (2006) are shown in Figure 9. While there may be a handful of such systems in our sample, the bulk of the ChESS stars are redder in $u-g$ than would be expected for systems with WD components.

To investigate the cause of this $u-g$ offset, Figure 10 also shows the magnitude of the $u-g$ offset as a function of L_X , L_X/L_{bol} , and $i-K_s$, a proxy for stellar temperature and mass. A slight tendency for the offset to increase with L_X/L_{bol} may be present, particularly when considering only stars of a given spectral type, but linear regression does not return a statistically significant correlation between the two variables. One would expect the $u-g$ excess to be most prominent for M stars, which typically have the highest activity and the lowest of quiescent UV flux, allowing contributions from the chromosphere to affect the stars’ $u-g$ most significantly. Instead, the $u-g$ excess reaches a maximum for K stars (at $i-K_s \sim 2.0$) and then decreases into the M regime. Whether this effect is real or the result of observational bias is hard to access, in part because of the increased uncertainties in $u-g$ for late-type stars caused by the red leak in the SDSS camera¹⁹. The additional scatter in the $u-g$ colors of these stars may wash out evidence for trends of $\delta(u-g)$ with either L_X or color. Follow-up studies with more reliable u photometry are needed to reveal the nature of any correlation between $u-g$ excess and coronal or chromospheric activity.

5.8. Stellar Populations

¹⁹ The red leak describes an instrumental effect whereby the u -band filter transmits flux longward of 7100 Å due to changes in the filter’s interference coating under vacuum. This instrumental effect depends on a star’s raw u and r magnitudes, which in turn are dependent on the airmass, seeing, and the sensitivity of each u filter as a function of wavelength and stellar spectrum. Given the complexity of this effect, the SDSS photometric pipeline does not attempt to correct each star’s u -band photometry, resulting in increased u uncertainties of 0.02 mag for K stars, 0.06 mag for M0 stars, and 0.3 mag for stars with $r-i > 1.5$. For more information see <http://www.sdss.org/dr6/products/catalogs/index.html>.

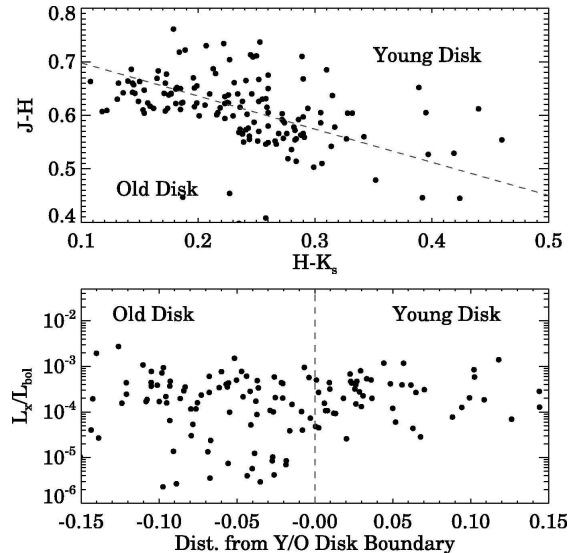


FIG. 12.— *Top Panel:* $J-H$ vs. $H-K_s$ for ChESS M stars with unflagged X-ray detections. The dashed line is the boundary between the regions identified by Stauffer & Hartmann (1986) and Leggett (1992) as populated preferentially on one side by relatively high-metallicity young disk stars and on the other by relatively low-metallicity old disk stars. *Bottom Panel:* L_X/L_{bol} as a function of offset in $J-H$ from the young disk/old disk boundary in the top panel.

Previous studies have found that magnetically active stars have a smaller Galactic scale height than non-active stars (e.g., West et al. 2008). To determine how the stars in our catalog are distributed between the different Galaxy components, we use each star’s distance and Galactic latitude to calculate its height in the Galactic disk. We show in Figure 11 the resulting Galactic heights as a function of both Galactic latitude and stellar color. If our catalog were probing a spherically symmetric halo population, the color-magnitude cut imposed in §4.4 would limit the catalog mainly as a function of the heliocentric distance to each star. Sight lines probing higher Galactic latitudes would sample stars at larger Galactic heights. The distribution of Galactic heights in the sample is independent of Galactic latitude, however, indicating that the distribution of stars within the disk of the Milky Way imposes a stricter distance limit than the color-magnitude cut imposed in §4.4.

Stauffer & Hartmann (1986) and Leggett (1992) have correlated the near-infrared colors of M stars and their metallicities and kinematics, allowing them to define regions of $J-H$ vs. $H-K_s$ color-color space dominated by young and old disk stars. In Figure 12, we compare the JHK_s colors of M stars in our sample to the boundary defined by Leggett (1992) between young and old disk stars. This boundary nearly bisects our sample, suggesting that the ChESS catalog contains both young stars and the high activity tail of the old disk population. Figure 12 also shows L_X/L_{bol} for these M stars as a function of their offset from the young/old disk boundary. The lowest activity sources ($L_X/L_{\text{bol}} \sim 10^{-5}$) are uniformly identified with the old disk population, a clear signature of the decay of magnetic activity with age. Interpreting the significance of the many old disk stars with large L_X/L_{bol} values is less straightforward, particularly be-

cause these active old disk stars are likely merely color outliers of the vastly more numerous young disk population. If these high L_X/L_{bol} stars are truly members of the old disk, however, they would represent a new and very significant population of stars that experience little decay of magnetic activity over their lifetimes.

6. CONCLUSIONS

We have correlated the Extended *Chandra* Multiwavelength Project with the Sloan Digital Sky Survey to identify the 348 X-ray emitting stars of the ChaMP Extended Stellar Survey. We used morphological star/galaxy separation, matching to an SDSS quasar catalog, an optical color-magnitude cut, and X-ray data quality tests to identify the ChESS stars from a sample of 2121 matched ChaMP/SDSS sources.

- Our cuts retain 91% of the spectroscopically confirmed stars in the original sample while excluding 99.6% of the 684 spectroscopically confirmed extragalactic sources. Fewer than 3% of the sources in our final catalog are previously identified stellar X-ray emitters.
- For 42 catalog members, spectroscopic classifications are available in the literature. We present new spectral classifications and $H\alpha$ measurements for an additional 79 stars. We derive distances to the stars in our catalog using photometric parallax relations appropriate for dwarfs on the main sequence and calculate their X-ray and bolometric luminosities. For 36 newly identified X-ray emitting M stars we also provide measurements of $L_{H\alpha}/L_{\text{bol}}$.
- The stars in our catalog lie in a unique space in the L_X -distance plane, filling the gap between the nearby stars identified as counterparts to sources in the *ROSAT* All-Sky Survey and the more distant stars detected in other *Chandra* and *XMM-Newton* surveys.
- The ChESS catalog is dominated by main sequence stars. By comparing the distribution of the ChESS sample in J vs. $J - K_S$ space to that of simulated SDSS/2MASS observations generated by TRILEGAL, we estimate that the total fraction of giants in the catalog is $\sim 10\%$. In addition to seven confirmed giant stars (including a possible Cepheid and an RR Lyrae star), we identify three cataclysmic variables.
- We find that $L_{H\alpha}/L_{\text{bol}}$ and L_X/L_{bol} are linearly related below $L_X/L_{\text{bol}} \sim 3 \times 10^{-4}$, while $L_{H\alpha}/L_{\text{bol}}$ appears to turn over at larger L_X/L_{bol} values.
- Stars with reliable SDSS photometry have an ~ 0.1 mag blue excess in $u - g$, likely due to increased chromospheric continuum emission. Photometric metallicity estimates suggest that our sample is evenly split between the young and old disk populations of the Galaxy; the lowest activity sources are identified with the old disk population, a clear signature of the decay of magnetic activity with age.

Future papers will present analyses of ChESS source variability and comparisons of the ChESS catalog to models of stellar activity in the Galactic disk.

We thank Suzanne Hawley, Andrew West, Steven Saar, and Thomas Fleming for useful discussions of stellar magnetic activity; we also thank the anonymous referee and editor for useful comments that improved the work presented here. We are indebted to the staffs at the National Optical Astronomy Observatories, Las Campanas, and the MMT for assistance with optical spectroscopy. Special thanks to observers including Warren Brown, Perry Berlind, and Michael Calkins, for FAST spectroscopy from the Fred Lawrence Whipple Observatory 1.5 m on Mt Hopkins, and to Susan Tokarz and Nathalie Marthimbeau for reductions.

Support for this work was provided by the National Aeronautics and Space Administration through *Chandra*, Award Number AR4-5017X and AR6-7020X issued by the *Chandra* X-ray Observatory Center, which is operated by the Smithsonian Astrophysical Observatory for and on behalf of the National Aeronautics Space Administration under contract NAS8-03060. Further NASA support was provided to K. Covey through the Spitzer Space Telescope Fellowship Program, through a contract issued by the Jet Propulsion Laboratory, California Institute of Technology under a contract with NASA. M. Agüeros is supported by an NSF Astronomy and Astrophysics Postdoctoral Fellowship under award AST-0602099. D. Haggard is supported by a NASA Harriett G. Jenkins Predoctoral Fellowship.

This work is based in part on observations obtained at Cerro Tololo Inter-American Observatory and Kitt Peak Observatory, National Optical Astronomy Observatory, operated by the Association of Universities for Research in Astronomy, Inc. under cooperative agreement with the National Science Foundation.

This research has made use of NASA's Astrophysics Data System Bibliographic Services, the SIMBAD database, operated at CDS, Strasbourg, France, the NASA/IPAC Extragalactic Database, operated by the Jet Propulsion Laboratory, California Institute of Technology, under contract with the National Aeronautics and Space Administration, and the VizieR database of astronomical catalogs (Ochsenbein et al. 2000). IRAF (Image Reduction and Analysis Facility) is distributed by the National Optical Astronomy Observatories, which are operated by the Association of Universities for Research in Astronomy, Inc., under cooperative agreement with the National Science Foundation.

Funding for the SDSS and SDSS-II has been provided by the Alfred P. Sloan Foundation, the Participating Institutions, the National Science Foundation, the U.S. Department of Energy, the National Aeronautics and Space Administration, the Japanese Monbukagakusho, the Max Planck Society, and the Higher Education Funding Council for England. The SDSS Web Site is <http://www.sdss.org/>.

The SDSS is managed by the Astrophysical Research Consortium for the Participating Institutions. The Participating Institutions are the American Museum of Natural History, Astrophysical Institute Potsdam, University of Basel, University of Cambridge, Case Western

Reserve University, University of Chicago, Drexel University, Fermilab, the Institute for Advanced Study, the Japan Participation Group, Johns Hopkins University, the Joint Institute for Nuclear Astrophysics, the Kavli Institute for Particle Astrophysics and Cosmology, the Korean Scientist Group, the Chinese Academy of Sciences (LAMOST), Los Alamos National Laboratory, the Max-Planck-Institute for Astronomy (MPIA), the Max-Planck-Institute for Astrophysics (MPA), New Mexico State University, Ohio State University, University of Pittsburgh, University of Portsmouth, Princeton Uni-

versity, the United States Naval Observatory, and the University of Washington.

The Two Micron All Sky Survey was a joint project of the University of Massachusetts and the Infrared Processing and Analysis Center (California Institute of Technology). The University of Massachusetts was responsible for the overall management of the project, the observing facilities and the data acquisition. The Infrared Processing and Analysis Center was responsible for data processing, data distribution and data archiving.

APPENDIX

CHAMP SOURCES WITH SIMBAD COUNTERPARTS

In Table A4 we present the optical data for the 66 stars cataloged in SIMBAD that we have identified as ChaMP X-ray sources, and include additional information (spectral type, binarity, variability) where available. We searched the literature for evidence that these stars had been identified as X-ray sources and could find no previous X-ray detections; we therefore consider these all to be new X-ray source identifications. Four stars are positionally coincident with X-ray sources in other *Chandra* catalogs, but are not explicitly listed in SIMBAD as X-ray emitters or identified in these catalogs as stars, and we therefore consider them also to be new identifications. CXOMP J084944.7+445840 is among the sources detected in Lynx (Stern et al. 2002) and listed in the Serendipitous Extragalactic X-Ray Source Identification (SEXSI; Harrison et al. 2003) catalog, but is unidentified in both catalogs. CXOMP J085005.3+445819 and J090941.7+541939 are both unidentified SEXSI sources. Finally, CXOMP J162157.2+381734 is less than 10'' from 1RXS J162157.6+381727, an unidentified RASS source.

13 ChaMP stellar sources do not have SIMBAD optical counterparts but are included in other X-ray catalogs. However, our examination of these catalogs reveals no additional information about the nature of these sources, and we also consider these to be new X-ray source identifications. For example, CXOMP J084854.0+450230 is within 1'' of the X-ray source [STS2002] 43 (Stern et al. 2002), but the catalog for that survey does not include an identification for this X-ray source or for two other ChaMP sources. Similarly, eight ChaMP sources listed in the SEXSI catalog and two observed in Bootes by Wang et al. (2004) are not identified. CXOMP J141120.7+521411 is included in three catalogs and unidentified in all three, although a magnitude is given for the counterpart by Zickgraf et al. (2003) in their catalog of RASS BSC sources. CXOMP J125152.2+000528 is listed by Zickgraf et al. (2003), but is unidentified. CXOMP J214229.3+123322 is within 4'' of the unidentified RASS source 1RXS J214229.5+123323. These sources are listed in Table A5. In total, we have 79 ChESS stars with cataloged optical or X-ray data, but which had not previously been identified as stellar X-ray sources.

Finally, 10 ChESS stars are previously known stellar X-ray sources. We list these in Table A6. A full examination of the properties of these stars (e.g., a comparison of their previously reported fluxes to those detected by *Chandra*) is beyond the scope of this paper.

REFERENCES

- Adelman-McCarthy, J. K. et al. 2007, *ApJS*, 172, 634
 Adelman-McCarthy, J. K., et al. 2008, *ApJS*, 175, 297
 Akerlof, C. et al. 2000, *AJ*, 119, 1901
 Aldcroft, T. L., Karovska, M., Cresitello-Dittmar, M. L., Cameron, R. A., & Markevitch, M. L. 2000, in Presented at the Society of Photo-Optical Instrumentation Engineers (SPIE) Conference, Vol. 4012, *Proc. SPIE* Vol. 4012, p. 650-657, X-Ray Optics, Instruments, and Missions III, Joachim E. Truemper; Bernd Aschenbach; Eds., ed. J. E. Truemper & B. Aschenbach, 650-657
 Alexander, D. M. et al. 2003, *AJ*, 126, 539
 Amado, P. J. 2003, *A&A*, 404, 631
 Amado, P. J., & Byrne, P. B. 1997, *A&A*, 319, 967
 Anderson, S. F., et al. 2007, *AJ*, 133, 313
 Apparao, K. M. V., Berthiaume, G. D., & Nousek, J. A. 1992, *ApJ*, 397, 534
 Bade, N., et al. 1998, *A&AS*, 127, 145
 Barkhouse, W. A. et al. 2006, *ApJ*, 645, 955
 Bochanski, J. J., West, A. A., Hawley, S. L., & Covey, K. R. 2007, *AJ*, 133, 531
 Brandt, W. N., & Hasinger, G. 2005, *ARA&A*, 43, 827
 Cappi, M. et al. 2001, *ApJ*, 548, 624
 Collier Cameron, A., & Jianke, L. 1994, *MNRAS*, 269, 1099
 Covey, K. R. et al. 2007, *AJ*, 134, 2398
 Cram, L. E. 1982, *ApJ*, 253, 768
 Cutri, R. M., et al. 2003, 2MASS All Sky Catalog of point sources. (The IRSA 2MASS All-Sky Point Source Catalog, NASA/IPAC Infrared Science Archive. <http://irsa.ipac.caltech.edu/applications/Gator/>)
 Della Ceca, R. et al. 2004, *A&A*, 428, 383
 Favata, F., Micela, G., Sciortino, S., & Vaiana, G. S. 1992, *A&A*, 256, 86
 Feigelson, E. D., et al. 2004, *ApJ*, 611, 1107
 Freyberg, M. J., Altieri, B., Bermejo, D., Esquej, M. P., Lazaro, V., Read, A. M., & Saxton, R. D. 2006, in *ESA Special Publication*, Vol. 604, *The X-ray Universe 2005*, ed. A. Wilson, 913+
 Fukugita, M., et al. 1996, *AJ*, 111, 1748
 Gehrels, N. 1986, *ApJ*, 303, 336
 Gioia, I. M., et al. 1984, *ApJ*, 283, 495
 —. 1990, *ApJS*, 72, 567
 Girardi, L. et al. 2005, *A&A*, 436, 895
 Green, P. J. et al. 2004, *ApJS*, 150, 43
 Gunn, J. E., et al. 1998, *AJ*, 116, 3040
 —. 2006, *AJ*, 131, 2332
 Hagen, H.-J., et al. 1995, *A&AS*, 111, 195
 Harris, D. E., & Johnson, H. M. 1985, *ApJ*, 294, 649
 Harrison, F. A., Eckart, M. E., Mao, P. H., Helfand, D. J., & Stern, D. 2003, *ApJ*, 596, 944
 Herbst, W., & Miller, J. R. 1989, *AJ*, 97, 891
 Hogg, D. W., et al. 2001, *AJ*, 122, 2129
 Houdebine, E. R., Mathioudakis, M., Doyle, J. G., & Foing, B. H. 1996, *A&A*, 305, 209
 Houdebine, E. R., & Stempels, H. C. 1997, *A&A*, 326, 1143

- Hünsch, M., Schmitt, J. H. M. M., Sterzik, M. F., & Voges, W. 1999, *A&AS*, 135, 319
- Ishisaki, Y., Ueda, Y., Yamashita, A., Ohashi, T., Lehmann, I., & Hasinger, G. 2001, *PASJ*, 53, 445
- Ivezić, Z., et al. 2004, *Astronomische Nachrichten*, 325, 583
- James, D. J., Jardine, M. M., Jeffries, R. D., Randich, S., Collier Cameron, A., & Ferreira, M. 2000, *MNRAS*, 318, 1217
- Jardine, M. 2004, *A&A*, 414, L5
- Karaali, S., Bilir, S., & Tunçel, S. 2005, *Publications of the Astronomical Society of Australia*, 22, 24
- Kim, D.-W. et al. 2006, *ApJ*, 644, 829
- . 2004a, *ApJS*, 150, 19
- . 2004b, *ApJ*, 600, 59
- Kim, M. et al. 2007a, *ApJS*, 169, 401
- Kim, M., Wilkes, B. J., Kim, D.-W., Green, P. J., Barkhouse, W. A., Lee, M. G., Silverman, J. D., & Tananbaum, H. D. 2007b, *ApJ*, 659, 29
- Kraus, A. L., & Hillenbrand, L. A. 2007, *AJ*, 134, 2340
- Lavalley, M., Isobe, T., & Feigelson, E. 1992, in *Astronomical Society of the Pacific Conference Series*, Vol. 25, *Astronomical Data Analysis Software and Systems I*, ed. D. M. Worrall, C. Biemesderfer, & J. Barnes, 245–+
- Leggett, S. K. 1992, *ApJS*, 82, 351
- Lehmann, I. et al. 2001, *A&A*, 371, 833
- López-Santiago, J., Micela, G., Sciortino, S., Favata, F., Caccianiga, A., Della Ceca, R., Severgnini, P., & Braito, V. 2007, *A&A*, 463, 165
- Mason, K. O. et al. 2000, *MNRAS*, 311, 456
- Mathioudakis, M., & Doyle, J. G. 1989, *A&A*, 224, 179
- Monet, D. G. et al. 2003, *AJ*, 125, 984
- Nieto-Santisteban, M. A., et al. 2004, in *ASP Conf. Ser.* 314: *Astronomical Data Analysis Software and Systems (ADASS) XIII*, ed. F. Ochsenbein, M. G. Allen, & D. Egret, 666–+
- Ochsenbein, F., Bauer, P., & Marcout, J. 2000, *A&AS*, 143, 23
- Parejko, J. K., Constantin, A., Vogeley, M. S., & Hoyle, F. 2008, *AJ*, 135, 10
- Pettersen, B. R. 1987, *Vistas in Astronomy*, 30, 41
- Pflueger, B., Otterbein, K., & Staubert, R. 1996, *A&A*, 305, 699
- Popesso, P., et al. 2004, *A&A*, 423, 449
- Randich, S., Schmitt, J. H. M. M., & Prosser, C. 1996, *A&A*, 313, 815
- Reid, N., Hawley, S. L., & Mateo, M. 1995, *MNRAS*, 272, 828
- Richards, G. T. et al. 2007, in *American Astronomical Society Meeting Abstracts*, Vol. 211, *American Astronomical Society Meeting Abstracts*, 142.02–+
- Richards, G. T. et al. 2004, *ApJS*, 155, 257
- . 2006, *AJ*, 131, 2766
- Saxton, R. D., Read, A. M., Esquej, P., Freyberg, M. J., Altieri, B., & Bermejo, D. 2008, *A&A*, 480, 611
- Schmitt, J. H. M. M., Golub, L., Harnden, Jr., F. R., Maxson, C. W., Rosner, R., & Vaiana, G. S. 1985, *ApJ*, 290, 307
- Schmitt, J. H. M. M., & Liefke, C. 2004, *A&A*, 417, 651
- Schmitt, J. H. M. M., et al. 1995, *ApJ*, 450, 392
- Scranton, R. et al. 2002, *ApJ*, 579, 48
- Silverman, J. D. et al. 2005, *ApJ*, 624, 630
- Silvestri, N. M. et al. 2006, *AJ*, 131, 1674
- Skrutskie, M. F. et al. 1997, in *ASSL Vol. 210: The Impact of Large Scale Near-IR Sky Surveys*, 25–+
- Skrutskie, M. F., et al. 2006, *AJ*, 131, 1163
- Smith, J. A., et al. 2002, *AJ*, 123, 2121
- Smolčić, V. et al. 2004, *ApJ*, 615, L141
- Stauffer, J. R., Caillault, J.-P., Gagne, M., Prosser, C. F., & Hartmann, L. W. 1994, *ApJS*, 91, 625
- Stauffer, J. R., & Hartmann, L. W. 1986, *ApJS*, 61, 531
- Stern, D. et al. 2002, *AJ*, 123, 2223
- Stocke, J. T., et al. 1983, *ApJ*, 273, 458
- . 1991, *ApJS*, 76, 813
- Stoughton, C., et al. 2002, *AJ*, 123, 485
- Sung, H., Bessell, M. S., Lee, B.-W., & Lee, S.-G. 2002, *AJ*, 123, 290
- Szkody, P., et al. 2003, *AJ*, 126, 1499
- . 2005, *AJ*, 129, 2386
- Vilhu, O. 1987, in *Lecture Notes in Physics*, Berlin Springer Verlag, Vol. 291, *Cool Stars, Stellar Systems and the Sun*, ed. J. L. Linsky & R. E. Stencel, 110–+
- Vilhu, O., & Rucinski, S. M. 1983, *A&A*, 127, 5
- Voges, W., et al. 1999, *A&A*, 349, 389
- . 2000, *VizieR Online Data Catalog*, 9029, 0
- Walkowicz, L. M., Hawley, S. L., & West, A. A. 2004, *PASP*, 116, 1105
- Wang, J. X. et al. 2004, *AJ*, 127, 213
- Watson, M., & XMM-Newton Survey Science Centre Consortium, t. 2006, in *Bulletin of the American Astronomical Society*, Vol. 38, *Bulletin of the American Astronomical Society*, 365–+
- Weinstein, M. A. et al. 2004, *ApJS*, 155, 243
- Weisskopf, M. C., Brinkman, B., Canizares, C., Garmire, G., Murray, S., & Van Speybroeck, L. P. 2002, *PASP*, 114, 1
- West, A. A., Hawley, S. L., Bochanski, J. J., Covey, K. R., Reid, I. N., Dhital, S., Hilton, E. J., & Masuda, M. 2008, *AJ*, 135, 785
- Woudt, P. A., et al. 2004, *MNRAS*, 351, 1015
- Woźniak, P. R. et al. 2004, *AJ*, 127, 2436
- Zickgraf, F.-J., et al. 2003, *A&A*, 406, 535

TABLE A1
CHAMP STELLAR CATALOG (X-RAYS)

Source (CXOMP)	Chandra Obs. ID	fBc (10^{-13} ergs cm^{-2} s^{-1})	netBc (counts)	fSc (10^{-13} ergs cm^{-2} s^{-1})	netSc (counts)	HR ^a	$\text{Log}(L_{Xs})$ (Log ergs s^{-1})	$\text{Log}(\frac{L_{Xs}}{L_{bol}})$	$\text{Log}(L_{Xb})$ (Log ergs s^{-1})	$\text{Log}(\frac{L_{Xb}}{L_{bol}})$
J000155.4+004819	4861	0.08± 0.08	3.5± 3.4	0.01± 0.03	0.6± 2.3	1.00	28.60± 1.30	-4.44± 1.30	29.60± 1.47	-3.45± 1.47
J001107.9+144153	3957	0.19± 0.10	7.7± 4.0	0.10± 0.05	7.9± 4.0	-1.00	28.34± 0.30	-3.07± 0.30	28.61± 0.31	-2.80± 0.31
J001313.2+000250	4829	0.10± 0.05	8.5± 4.1	0.05± 0.02	7.8± 4.0	-1.00	29.08± 0.31	-4.40± 0.31	29.41± 0.29	-4.07± 0.29
J003151.4+003233	2101	0.59± 0.12	34.7± 7.0	0.29± 0.06	33.9± 6.9	-0.90	28.27± 0.10	-3.45± 0.10	28.59± 0.10	-3.13± 0.10
J004238.8-091043	4886	0.97± 0.13	66.4± 9.2	0.54± 0.08	62.6± 9.0	-0.93	29.73± 0.07	-3.11± 0.07	29.98± 0.07	-2.86± 0.07
J010615.6+004814	2180	0.36± 0.11	16.5± 5.2	0.18± 0.06	15.9± 5.1	-0.81	28.73± 0.17	-3.31± 0.17	29.03± 0.16	-3.01± 0.16
J011818.5-005642	4963	0.14± 0.03	36.0± 8.5	0.09± 0.02	37.5± 7.6	-1.00	29.25± 0.10	-3.43± 0.10	29.44± 0.12	-3.23± 0.12
J014821.7+000446	4098	0.09± 0.07	4.0± 3.2	0.04± 0.03	3.0± 2.9	-0.71	28.31± 1.67	-3.11± 1.67	28.73± 0.69	-2.70± 0.69
J015939.2-084409	6106	0.01± 0.02	2.2± 4.3	0.01± 0.01	6.2± 4.0	-1.00	27.06± 0.44	-5.57± 0.44	26.85± 1.30	-5.79± 1.30
J015941.6-084506	6106	0.11± 0.03	31.1± 7.1	0.07± 0.01	30.5± 6.7	-1.00	27.82± 0.11	-5.11± 0.11	28.05± 0.11	-4.88± 0.11
J015959.7+003220	5777	0.75± 0.08	115.2± 12.6	0.40± 0.04	103.3± 11.5	-0.88	28.91± 0.05	-3.57± 0.05	29.18± 0.05	-3.29± 0.05
J020643.7+121851	3029	0.14± 0.06	9.3± 4.3	0.06± 0.03	7.8± 4.0	-0.80	28.15± 0.31	-3.15± 0.31	28.52± 0.27	-2.78± 0.27
J022429.5-000020	4987	0.04± 0.01	43.5± 8.0	0.02± 0.00	40.3± 7.5	-0.91	27.75± 0.09	-3.66± 0.09	28.07± 0.09	-3.34± 0.09
J022437.7-000711	4987	0.04± 0.01	31.0± 6.9	0.02± 0.00	31.9± 6.8	-1.00	28.15± 0.10	-4.00± 0.10	28.38± 0.11	-3.77± 0.11

^aSince we do not include any scientific results based on HR, we simply characterize the typical errors here by noting that the mean error on HR is well-fit for sources with HR > -0.98 by $\text{HR}_{\text{err}} = 0.36(\pm 0.027) * HR + 0.40(\pm 0.022)$, with RMS residuals of $\sigma=0.074$. Sources with HR < -0.98 have median HR errors of 0.106, with RMS residuals of $\sigma=0.073$.

TABLE A2
CHAMP STELLAR CATALOG (OPTICAL/IR)

Source	SDSS dist (")	<i>i</i> (mag)	<i>u - g</i> (mag)	<i>g - r</i> (mag)	<i>r - i</i> (mag)	<i>i - z</i> (mag)	Syn. <i>g</i> (mag)	Sat. (Flag)	<i>J</i> (mag)	<i>J - H</i> (mag)	<i>H - K_s</i> (mag)
J000155.4+004819	5.58	14.20± 0.01	1.41± 0.03	0.55± 0.02	0.20± 0.02	0.07± 0.03	15.47± 0.30	1	13.24± 0.02	0.38± 0.03	0.07± 0.04
J001107.9+144153	0.72	17.16± 0.01	2.02± 0.23	1.51± 0.03	1.63± 0.02	0.89± 0.02	20.49± 0.30	0	14.72± 0.03	0.65± 0.05	0.26± 0.07
J001313.2+000250	0.47	12.56± 0.01	1.17± 0.01	0.31± 0.01	0.10± 0.01	-0.01± 0.03	13.42± 0.30	1	11.73± 0.03	0.24± 0.04	0.04± 0.04
J003151.4+003233	0.87	14.97± 0.03	2.32± 0.06	1.49± 0.03	1.46± 0.03	0.79± 0.03	17.91± 0.30	0	12.70± 0.02	0.56± 0.04	0.28± 0.04
J004238.8-091043	0.24	13.36± 0.01	1.85± 0.07	-2.25± 0.07	3.22± 0.02	0.14± 0.02	14.82± 0.30	1	12.14± 0.02	0.45± 0.04	0.13± 0.04
J010615.6+004814	0.23	15.75± 0.03	2.48± 0.08	1.40± 0.04	1.24± 0.04	0.67± 0.03	18.26± 0.30	0	13.61± 0.03	0.60± 0.04	0.23± 0.04
J011818.5-005642	1.61	15.28± 0.02	2.35± 0.04	1.15± 0.04	0.52± 0.03	0.31± 0.03	17.25± 0.30	0	13.72± 0.02	0.61± 0.04	0.16± 0.04
J014821.7+000446	1.10	18.10± 0.01	2.40± 0.80	1.62± 0.05	1.58± 0.03	0.82± 0.03	20.70± 0.30	0	15.77± 0.07	0.76± 0.10	0.18± 0.13
J015939.2-084409	1.40	15.18± 0.02	2.64± 0.03	-0.96± 0.04	-0.54± 0.04	3.62± 0.02	13.76± 0.30	1	10.41± 0.02	0.62± 0.04	0.16± 0.03
J015941.6-084506	0.33	10.18± 0.01	1.87± 0.01	0.82± 0.01	0.30± 0.01	-1.97± 0.02	11.82± 0.30	1	9.34± 0.02	0.41± 0.06	0.09± 0.06
J015959.7+003220	1.32	13.86± 0.01	2.24± 0.03	1.43± 0.02	1.36± 0.01	0.73± 0.02	15.42± 0.30	1	11.72± 0.02	0.64± 0.03	0.25± 0.03
J020643.7+121851	0.52	17.59± 0.02	2.45± 0.50	1.63± 0.04	1.61± 0.03	0.88± 0.02	20.84± 0.30	0	15.20± 0.04	0.65± 0.06	0.39± 0.08
J022429.5-000020	0.43	17.50± 0.02	2.62± 0.56	1.46± 0.05	1.67± 0.03	0.87± 0.03	20.45± 0.30	0	15.15± 0.04	0.68± 0.06	0.31± 0.08
J022437.7-000711	0.85	16.14± 0.02	2.71± 0.12	1.41± 0.03	1.06± 0.03	0.58± 0.03	18.94± 0.30	0	14.10± 0.03	0.57± 0.04	0.27± 0.05

TABLE A3
 CHAMP STARS WITH SPECTRA.

CXOMP	Type	H α EqW (Å)	log L _{Hα} /L _{bol}
J001107.9+144153	M5	+6.09	-3.78
J001313.2+000250	F7	-3.67	...
J003151.4+003233	M4	+5.01	-3.50
J010615.6+004814	M3	+2.71	-3.70
J011818.5-005642	K5	+0.71	...
J015941.6-084506 ^a	K2	-1.76	...
J020643.7+121851	M5	+6.07	-3.78
J022429.5-000020	M4	+3.43	-3.66
J023206.6-073032	M4	+2.75	-3.76
J025951.7+004619 ^b	M5	+14.47	-3.40
J030014.0+004729	K1	-1.52	...
J072501.4+371351 ^a	K3	-1.15	...
J074108.8+311346 ^a	M6	+1.24	-4.66
J074112.3+311446	M4	+8.60	-3.26
J074118.8+311434	M3	+3.53	-3.58
J074433.8+393027	F2	-3.55	...
J074437.0+392503	M5	+5.71	-3.81
J074444.6+392931	F5	-3.69	...
J074705.1+274006	G1	-2.53	...
J075549.9+405728	M2	+0.09	-5.08
J075937.3+300846	G7	-0.88	...
J080046.6+360416	M2	-0.05	...
J080048.1+360722	F1	-3.54	...
J080101.0+360549	G2	-2.57	...
J080157.1+441438	K2	-0.74	...
J082702.2+291531	G4	-0.94	...
J082718.9+291841	M0	-0.45	...
J082726.2+291601	G2	-1.50	...
J082729.8+291905	K2	-1.11	...
J082815.2+291132	G5	-2.25	...
J084039.0+130916	M0	-0.30	...
J084044.7+130713 ^a	G1	-2.78	...
J084055.8+130800	M4	+2.97	-3.72
J084913.8+444758	M0	-0.42	...
J085325.7+232919 ^a	M4	+6.47	-3.39
J091047.6+541505	M2	+2.62	-3.60
J091104.1+542208	M2	-0.52	...
J093411.0+551143	F4	-4.09	...
J111504.7+403706	M3	+1.04	-4.12
J111802.3+074325	G0	-2.88	...
J112045.7+232536	M2	+3.67	-3.45
J112116.2+232622	M3	+0.17	-4.90
J114007.3+660659	M2	+2.43	...
J114101.7+661246	M3	+0.80	-4.23
J114129.7+660250	K3	-1.29	...
J114149.5+661123	K7	-0.31	...
J120439.4-001650	G8	-1.98	...
J122155.2+490743	M4	+4.79	-3.52
J122738.8+442132	M4	+3.28	-3.68
J122837.1+015720 ^b	M1	+1.19	...
J125152.2+000528	M3	+5.23	-3.41
J131231.0+423106	M3	+2.47	-3.74
J134433.5-000536	M4	+7.23	-3.34
J134434.8+554956	M3	+3.95	-3.53
J134449.1+555812	F8	-1.81	...
J134521.5-000118	M3	+2.43	-3.75
J140654.3+340949	M4	+3.81	-3.62
J141120.7+521411	K7	-0.94	...
J141715.2+445420	G7	-1.86	...
J144553.5+012552	M0	+0.55	-4.20
J150639.4+521856	M6	+3.43	-4.22
J151031.7+074248	K2	-0.07	...
J151423.8+363511	M3	+1.35	-4.00
J153245.2-004012	G8	-1.97	...
J153519.7+233152	M2	-0.32	...
J154905.1+213319	K3	-1.23	...
J154947.2+212857	G3	-2.57	...
J161958.8+292321	M2	+3.56	-3.46
J162306.8+311236	M4	+3.85	-3.61
J162415.4+263728	K2	-0.90	...
J214218.8+122524	G2	-1.72	...
J214229.3+123317	M2	+3.63	-3.45
J214229.3+123322	M4	+13.54	-3.06
J214235.6+122701	K0	-1.83	...
J221513.1-004828	M2	+1.39	-3.87
J221513.2-004927	G4	-2.77	...
J221516.8-005129	M4	+5.51	-3.46
J221716.9+002208	K5	-1.04	...

TABLE A4
CHAMP SOURCES WITH SIMBAD COUNTERPARTS.

CXOMP	SIMBAD Counterpart	Sep. (")	<i>B</i> (mag)	<i>V</i> (mag)	Comments
J015941.6-084506	BD-09 375	0.4	11.90	10.80	...
J015959.7+003220	[BHR2005] 829-29	1.8	M3.5V
J023132.5-072724	TYC 4704-81-1	1.1	11.70	11.20	...
J025951.7+004619	[BHR2005] 832-7	0.0	M5.5V
J072501.4+371351	TYC 2464-396-1	0.9	10.55	9.52	...
J072545.4+365905	BD+37 1715	0.6	10.72	10.28	F5
J074108.8+311346	2MASS J07410881+3113463	0.0	19.20
J080500.8+103001	HD 66686	1.9	8.17	7.29	G5III
J080853.8+201641	BD+20 2009	2.3	10.86	10.60	F5
J080920.5+202322	BD+20 2011	1.2	10.82	10.14	F0
J081539.2+364742	TYC 2482-1192-1	1.7	11.70	11.10	...
J084044.7+130713	TYC 805-471-1	1.2	11.80	11.20	...
J084944.7+445840 ^{a,b}	HD 75117	0.8	8.45	7.98	G0
J085005.3+445819 ^b	HD 75172	4.2	9.24	8.98	F5
J085318.2+281106	TYC 1949-1327-1	1.5	11.20	10.39	...
J085325.7+232919	2MASS J08532577+2329194	1.1
J085711.0+085651	TYC 811-1921-1	2.6	11.10	10.70	...
J090941.7+541939 ^b	TYC 3805-167-1	2.5	10.95	10.50	...
J091432.7+561238	HD 237796	0.6	10.65	9.61	K5
J091444.7+562104	TYC 3809-904-1	1.8	11.40	10.90	...
J093342.5+340154	TYC 2497-1154-1	0.8	11.70	11.30	...
J093905.4+005146	TYC 235-1240-1	2.1	11.50	11.00	...
J095427.2+410515	BD+41 2023	1.7	11.10	10.36	K0
J095721.0+465821	TYC 3433-1205-1	2.0	11.60	10.90	...
J103857.9+400335	TYC 3005-806-1	1.3	10.50	10.22	...
J104320.6+005954	TYC 254-1148-1	3.3	11.90	11.10	...
J105202.9+160544	CCDM J10520+1606AB	0.6	8.68	8.31	F5 **
J105211.8+161002	BD+16 2181	0.9	9.93	9.66	F5
J111446.9+532038	TYC 3824-287-1	1.2	11.19	10.71	...
J111548.9+532234	2MASS J11154905+5322345	1.4	12.80
J111607.3+013512	CCDM J11161+0135AB	0.8	9.48	9.01	F8 **
J111607.3+013509	CCDM J11161+0135AB	3.2	9.48	9.01	F8 **
J114144.3+654114	HD 101557	1.5	9.65	8.97	G5
J115931.2+553109	GPM 179.879716+55.519459	1.2	12.00	11.50	...
J120041.3+290512	BD+29 2244	4.1	11.08	10.57	F6
J120154.0+575636	HD 104482	0.9	9.48	9.02	F5
J120205.1+575539	HD 238063	0.4	10.37	9.97	F5
J124533.5+005914	HD 110935	1.5	9.98	9.08	G5
J125152.0+000505	HD 111816	1.0	8.31	7.83	F8
J125605.1+260117	BD+26 2407	2.3	10.09	9.73	F2
J125615.7+564817	GSC 03845-00748	1.2	12.50
J130115.9+002958	NLTT 32614	2.6	10.45	9.59	K0 PM*
J130549.6+035341	LSPM J1305+0353	0.4	18.80	...	PM*
J130908.5+212721	CCDM J13091+2127AB	0.9	8.93	8.34	G5 **
J130955.3+573403	HD 114505	1.1	9.80	9.21	G
J131043.9-031731	HD 114465	0.7	9.12	8.71	F8
J131057.7+011553	StKM 1-1052	3.2	...	11.40	K5
J133143.4+111132	BD+11 2580	0.7	11.00	9.96	K0
J141345.7+000710	2MASS J14134569+0007068	2.8	18.96
J141349.2+000806	2MASS J14134944+0008055	3.5	15.97
J141808.1+264743	HD 125320	0.8	8.93	8.19	G5IV
J143800.1+033528	HD 128645	0.5	9.72	9.40	F5
J144232.8+011710	BD+01 2965	0.7	10.41	9.10	K0III
J144300.8+012423	2MASS J14430071+0124239	1.8	15.30
J144430.1-012826	2MASS J14443011-0128261	0.3	15.30	15.29	RR*
J144848.7+474041	GSC 03477-01108	1.1	14.00
J152209.8+524435	HD 137146	1.9	9.70	9.26	F8
J153203.6+240505	BD+24 2880	0.8	9.86	9.42	F8
J153658.6+120011	GPM 234.244393+12.002844	0.7	12.40	11.30	...
J160234.6+423021	HD 144129	0.6	9.85	9.46	F5
J162157.2+381734 ^c	TYC 3062-1317-1	0.2	11.80	10.50	Ce* ^d
J162357.2+311253	TYC 2580-796-1	0.7	11.70	11.50	...
J170137.9+400548	TYC 3076-801-1	3.0	10.93	10.11	...
J171952.9+263003	NLTT 44615	1.0	13.80	13.60	PM*
J231820.3+003129	HD 219752	1.1	9.54	9.11	F5
J231956.4+003418	TYC 577-673-1	1.0	11.90	11.20	...

NOTE. — “**” indicates a double or multiple star, “PM*” indicates a high proper motion stars, “RR*” a RR Lyr-type variable, and “Ce*” a Cepheid-type variable.

^aSource cataloged in Stern et al. (2002).

^bSource cataloged in Harrison et al. (2003).

^cSource cataloged in Voges et al. (2000).

^dWhile this star is classified as a Cepheid by Akerlof et al. (2000), inspection of the Northern Sky Variability Survey (Woźniak et al. 2004) lightcurve for this object suggests that this is not a classical Cepheid.

TABLE A5
CHAMP SOURCES INCLUDED IN OTHER X-RAY CATALOGS.

CXOMP	Other Name	Sep. (")	Catalog
J084854.0+450230	[STS2002] 43	1.1	Stern et al. (2002)
	CXOSEXSI J084854.0+450231	1.4	Harrison et al. (2003)
J084913.8+444758	[STS2002] 88	1.8	Stern et al. (2002)
J084921.3+444949	CXOSEXSI J084921.2+444948	0.5	Harrison et al. (2003)
	[STS2002] 106	0.9	Stern et al. (2002)
J091045.7+542019	CXOSEXSI J091045.7+542019	2.9	Harrison et al. (2003)
J091047.6+541505	CXOSEXSI J091047.6+541505	0.8	Harrison et al. (2003)
J091104.1+542208	CXOSEXSI J091104.2+542206	1.9	Harrison et al. (2003)
J115903.8+291747	CXOSEXSI J115903.7+291746	1.3	Harrison et al. (2003)
J125152.2+000528	[ZEH2003] RX J1251.8+0005 1	3.2	Zickgraf et al. (2003)
J141120.7+521411	CXOSEXSI J141120.7+521411	0.2	Harrison et al. (2003)
	[CME2001] 3C 295 12	1.0	Cappi et al. (2001)
	[ZEH2003] RX J1411.3+5212 1	1.4	$B = 14.1$; Zickgraf et al. (2003)
J142527.4+352656	CXOLALA1 J142527.5+352656	1.6	Wang et al. (2004)
J142547.1+353954	CXOLALA1 J142547.1+353954	0.9	Wang et al. (2004)
J162415.4+263728	CXOSEXSI J162415.4+263729	1.2	Harrison et al. (2003)
J214229.3+123322	1RXS J214229.5+123323	3.3	Voges et al. (2000)

TABLE A6
PREVIOUSLY KNOWN STELLAR X-RAY SOURCES WITH CHAMP DETECTIONS.

CXOMP	SIMBAD Counterpart	Sep. (")	B (mag)	V (mag)	Comments
J080813.5+210608	LHS 5134	0.5	12.65	11.20	M2.5 PM*; Hünsch et al. (1999)
J100734.8+130144	NLTT 23457	3.6	8.98	8.40	F8 PM*; Stocke et al. (1991)
J105336.4+573800	TYC 3829-162-1	0.6	11.00	10.43	Ishisaki et al. (2001) ^a
J105410.3+573038	RDS 20C	0.8	M5V; Ishisaki et al. (2001)
J122156.1+271834	HD 107611	0.9	8.95	8.50	F6V *iC; Randich et al. (1996)
J122837.1+015720 ^b	GSC 00282-00187	3.6	M2; Pflueger et al. (1996)
J125533.7+255331	PN G339.9+88.4	0.8	9.65	8.86	G5III PN; Apparao et al. (1992)
J134513.3+555244	NLTT 35142	1.8	6.97	6.50	F7IV-V PM*; Schmitt et al. (1985)
J135608.7+183039	GSC 01470-00791	1.4	...	15.00	K5; Mason et al. (2000)
J171954.1+263003	V* V647 Her	1.4	12.98	11.42	M4 Fl*; Harris & Johnson (1985)

NOTE. — "PM*" indicates a high proper motion stars, "*iC" a star in a cluster, "PN" a planetary nebula, "Ce*" a Cepheid-type variable, and "Fl*" a flare star.

^aBoth TYC 3829-162-1 and its probable X-ray counterpart, RX J105336.4+573802 (detected by Lehmann et al. (2001)), are listed in Ishisaki et al. (2001). This is presumably an accounting error.

^bAlso included in the López-Santiago et al. (2007) sample.